minerals

MDPI

Article

Granitoids of the Ergelyakh Intrusion-Related Gold–Bismuth Deposit (Kular-Nera Slate Belt, Northeast Russia): Petrology, Physicochemical Parameters of Formation, and Ore Potential

Albert I. Zaitsev, Valery Yu. Fridovsky * and Maxim V. Kudrin

Diamond and Precious Metal Geology Institute, SB RAS, Yakutsk 677000, Russia;
a.i.zaitsev@diamond.ysn.ru (A.I.Z.); kudrinmv@mail.ru (M.V.K.)
* Correspondence: 710933@list.ru; Tel.: +7-4112-33-58-72

Received: 17 January 2019; Accepted: 8 May 2019; Published: 15 May 2019

Abstract: This paper describes features of petrographic and chemical compositions and isotopic dating of the Ergelyakh and Sokh plutons, located within the Kular-Nera slate belt, Verkhoyansk-Kolyma folded region (VKFR), Northeast Russia. Intrusion of the massifs took place approximately 145–150 million years ago. Different isotopic systems on the whole rock samples and mineral separates record at least two stages of later tectono-magmatic activity 130–120 and 110–100 million years ago. Granitoid magmas for the Ergelyakh and Sokh plutons were formed at high temperatures (950–1060 °C) within the amphibolitic lower crust of an island arc setting. The ages of crustal protoliths for granitoids of the Ergelyakh intrusion-related gold–bismuth deposit, calculated on Rb–Sr and Sm–Nd two-stage models, are 1109–1383 and 1199–1322 million years, respectively. Formation of the Ergelyakh and Sokh plutons took place within a significant temperature interval (<450 to 901 °C) and, with regard to the superposition of later events, lasted for a long time. During the cooling process of granitoid melts, at the time of biotite crystallization in both massifs, a significant increase of oxygen fugacity was registered. The ore potential of granitoids of both massifs seems to be similar, but due to some differences in the physicochemical parameters of their formation (redox conditions), it was partially realized only within the Ergelyakh massif with the generation of several minor intrusion-related gold–bismuth deposits. Granitoid melts of the Ergelyakh massif were formed in relatively heterogeneous and oxidizing conditions (ΔNi–NiO = +3.26 to −3.60). Granitoid melts for the Sokh massif (ΔNi–NiO = −2.88 to −9.27) were formed in reducing conditions.

Keywords: granitoids; isotopic age; physicochemical parameters of formation; Ergelyakh and Sokh plutons; intrusion-related gold–bismuth deposit

1. Introduction

Intrusion-related gold deposits are widespread in Northeast Russia [1–10]. These include both large deposits with gold ore resources and reserves exceeding 50 t (Chepak, Teutedjak, Chistoe), and numerous deposits of smaller size (Dubach, Nenneli, Delyankir, Chuguluk, Levo-Dybinskoe, Kurum, Ergelyakh) [1]. Gold deposits of this type were first recognized in the Tintina gold belt in Alaska and the Yukon in the 1990s [11–18]. The most economically important deposits of the belt include Fort Knox, Pogo, and Dublin Gulch, among others [18].

Geology, mineralogy, pressure and temperature conditions of ore formation, and the sources of hydrothermal fluids of intrusion-related gold–bismuth deposits of the Verkhoyansk-Kolyma folded region are extensively discussed in [1–10,19,20] and references therein. The intrusion-related gold–bismuth mineralization is localized in small stocks of S- and I-type ilmenite series granitoids and/or adjacent hornfels

haloes, or in dikes of varying composition (granite–porphyry, porphyrite, lamprophyre, diabase) [2,6,21]. Mineralogically, the deposits can be classified into the bismuth–sulfotelluride–quartz (Levo-Dybinskoe, Kular, Ergelyakh, Tuguchak, Basugunya), bismuth–arsenide–sulfoarsenide (Myakit, Chepak, Dubach, Chistoe, Kandidatskoe), and bismuth–siderite–polysulfide (Arkachan) types [7]. The average gold grade of the deposits varies from 2 to 5 g/t.

This paper first discusses physicochemical parameters of the emplacement of granitoids of the Ergelyakh area related with gold–bismuth deposits, which are very important in evaluating its ore potential. Magmatism of the Ergelyakh gold area (EGA) is poorly studied and its genetic relationship to mineralization is unclear. Here we compare and contrast two plutons from the EGA belt, one (the Ergelyakh massif) mineralized and the other (the Sokh stock) not, to try to understand what aspects of the magmas that formed these two plutons might have controlled mineralization.

2. Methods

Samples were prepared for analysis using standard crushing and grinding procedures [22,23]. Mineral grains were separated by magnetic and density separation, with final sorting under a binocular microscope to remove altered grains and other accidental minerals, and were ground to 200 mesh. All analyses were performed at the Diamond and Precious Metal Geology Institute (DPMGI), Siberian Branch, Russian Academy of Sciences, Yakutsk. Chemical compositions of the rocks and minerals were determined by classical wet chemistry analysis. Other methods included spectrometry, atomic-emission spectrometry, ionometry with ion-selective electrode, gravimetry, and titrimetry.

Trace elements (Cr, Ni, V, Co, Se, Ba, Sr, Nb, Zr, Y, and Yb) were determined on a PGS-2 spectrograph equipped with a multichannel atomic-emission spectral analyzer (MCA). The MCA is designed to analyze elemental composition of samples by concurrently performing multi-channel registration. A sample mixed a refractory buffer evaporates from the carbon electrode channel filled with an internal standard. Buffer is used to prevent the effect of the sample composition on the analytical results. Buffer for the atomic-emission analysis of the volatile elements represents a mixture of seven weight fractions of Al_2O_3 three fractions of $CaCO_3$, one fraction of K_2CO_3, and 0.02% Bi_2O_3. Buffer for carbonates consists of five weight fractions of Al_2O_3, four fractions of SiO_2, one fraction of K_2CO_3, and 0.02% Bi_2O_3. It is prepared in the same way as for silicates. Standards and samples are diluted with buffer in the optimum weight ratio of 1:2. Buffer for the iron-group elements represented 0.05% internal standard mixed with carbon powder. Carbon powder provides a uniform evaporation of the sample. The weight ratio of the buffer and sample is 1:1. Based on the results of burning the standards, diagrams are constructed which aid in determining the contents of the elements analyzed. To correct variations in the spectrum position we used reference lines (Pd 302.79 nm and 342 nm).

Electron microprobe analysis was performed using a Camebax microanalyzer (Cameca, Courbevoie, France) and a Jeol JSM-6480LV scanning microscope (JEOL, Tokyo, Japan). Chemical compositions and characteristics of minerals and rocks of the studied samples are shown in Tables 1–5.

Rb–Sr isotope studies were made with a MI-1201-T mass spectrometer (Electron optics, Sumy, Ukraine) in single beam mode using tantalum ribbons. Rb concentrations were calculated by isotope dilution, and those of Sr by double isotope dilution. Sr isotope composition was estimated without adding an indicator. Chemical treatment of samples included decomposition in a mixture of NF + $HClO_4$ (3:1) in Teflon bombs in autoclave mode at a temperature of 200 °C for 8 h. Elements were separated by the ion-exchange chromatography method with the use of Dowex resin, 50 × 8, 200 mesh. The error in measuring the isotope ratios did not exceed 0.05%. Reproducibility for ^{87}Rb, ^{86}Sr, and the $^{87}Sr/^{86}Sr$ ratio was 0.5, 0.4, and 0.03%, respectively. The blank tests for the laboratory contamination showed 0.007–0.013 g/t Rb and 0.02–0.05 g/t Sr. The accuracy and reproducibility of isotope measurements were controlled by the isotope standard carbonate-70 with an average normalized $^{87}Sr/^{86}Sr$ value of 0.7089 ± 0.0002. In the analyses we used reagents of very high purity, which were additionally purified when necessary. The composition of feldspars from the EGA granitoids was studied using a combination of methods. We made a full silicate analysis of bulk

fractions of K-feldspar and plagioclase and of some specific gravity fractions of plagioclase. For one of the granodiorite samples, mineral composition was determined with the use of a Jeol JSM-6480LV scanning microscope (JEOL, Tokyo, Japan). Results of isotopic dating of granitoids are shown in Table 6.

The parameters of the physicochemical conditions of the EGA granitoid fosenations were estimated from both the whole rock and the mineral components using the programs described in [24–34].

3. Geology of the Study Areas

3.1. Geology of the Southeastern Part of the Kular-Nera Slate Belt

Granitoids of the Ergelyakh intrusion-related gold–bismuth deposit (EIRGD) are located near the Adycha-Taryn fault (AT) in the Kular-Nera slate belt (Figure 1) [6,35,36]. The fault separates the Kular-Nera slate belt from the Verkhoyansk fold-and-thrust belt. It is traced in a northwesterly direction and controls the distribution of orogenic gold (Sana, Drazhnoe, Levoberezhnoe, Pil', Malo-Tarynskoe, Yakutskoe), intrusion-related Au–Bi (Ergelyakh), gold–antimony (Sarylakh, Maltan, Tan), tin–tungsten (Bekkemskoe, Rep-Yuryue, Baryllyalakhskoe), and silver (Veshnee) deposits (Figure 1). The deposits were formed at different stages of the tectono-magmatic history of the region [35–38]. The Late Jurassic–Early Cretaceous time was marked by the collision of the Siberian craton and the Kolyma-Omolon microcontinent accompanied by folding and faulting, intrusion of S- and I-type granitoids, and formation of orogenic Au and intrusion-related Au–Bi and Sn–W deposits. Post-accretionary tectonic events, small granitoid stocks, subvolcanic granite porphyry dikes, and Au–Sb, Ag–Sb, and Ag deposits were related to Late Cretaceous subduction in the Okhotsk-Chukotka arc.

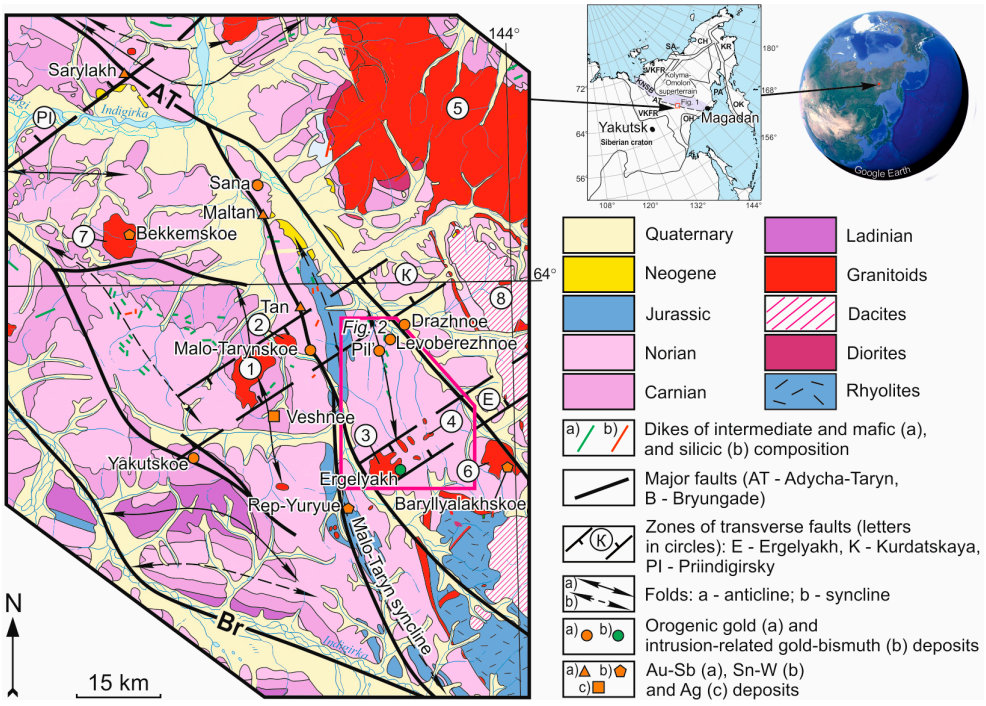

Figure 1. Location of Ergelyakh intrusion-related gold–bismuth deposit in the southeastern Kular-Nera slate belt. Circled figures: 1, Samyr; 2, Kurdat; 3, Ergelyakh; 4, Sokh; 5, Nelkan; 6, Baryllyalakh; 7, Kuranakh-Sala; 8, Taryn subvolcano. Inset shows (modified after [39]): Orogenic belts: SA, South Anyuy; PA, Penzha-Anadyr; Ch, Chukotka; KR, Koryak; OK, Olyutora-Kamchatka; VKFR, Verkhoyansk-Kolyma folded region; KNSB, Kular-Nera slate belt; OH, Okhotsk terrain. The red frame shows the position of Figure 2.

Various magmatic bodies are found in the fault zone, including dolerite, andesite, diorite porphyry, and basalt dikes, and small granitoid plutons, of which the largest are the Ergelyakh, Sokh, Kurdat, Samyr, and Saryllakh massifs (from SE to NW) forming ore clusters [40–45]. A series of intrusive granitoid bodies of the EIRGD extend northeasterly across the fold structures following the strike of the Ergelyakh transverse fault (Figures 1 and 2) [6]. The massifs are located in the eastern limb of the Malo-Taryn syncline. The largest is the Ergelyakh massif (50 km^2). Other plutons are no larger than 2 km^2, including the Sokh stock, about 1.7 km^2 in area. Some massifs form a single granodiorite–granite body at depth. The granitoids intrude into the Norian and Carnian sedimentary formations, which are metamorphosed to biotite and biotite–cordierite hornfels in exocontact zones of the plutons. The Carnian rocks include sandstones, siltstones, and clay shales. The Norian deposits are divided into the lower (sandstones and shales) and upper (shales and siltstones) substages. The alteration of the rocks is represented by greisenization.

The Ergelyakh massif has a zonal structure. Granodiorites (42%) make up the periphery of the massif, adamellites (20%) its apical part, and leucocratic granites (38%) the core. Dikes and veins of aplitic granites and aplites are widely developed, and pegmatite bodies occur locally. Relationships between various rock types of the massif are not well understood. Both sharp contacts and gradual transitions are observed.

The Sokh massif is composed of granodiorite porphyries intruded by leucocratic granites with an aplitic margin [6]. The aplite veins in the granodiorites of the massif transect quartz veinlets and are in turn cut by them. Between the Ergelyakh and Sokh massifs there are widespread dikes and veins of leucocratic and aplitic granites and aplites.

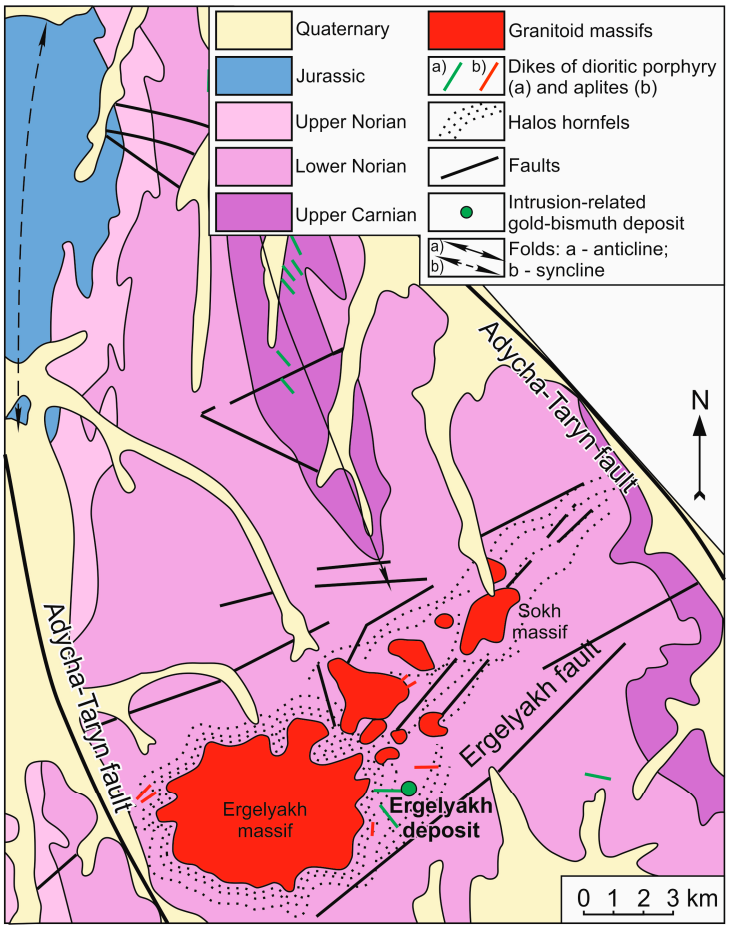

Figure 2. Geologic map of the area of the Ergelyakh and Sokh massifs, including the Ergelyakh intrusion-related gold–bismuth deposit.

3.2. Petrography of Igneous Rock of the Ergelyakh and Sokh Massifs

Granitoids of the Ergelyakh massif are represented by light gray equigranular rocks with a grain size up to 0.5 cm. They have a hypidiomorphic granular texture with elements of porphyritic texture (Figure 3A). The mineral contents of the granodiorites are plagioclase (42–60%), orthoclase (8–19%), quartz (17–35%), and biotite (7.5–16%). Plagioclase is present as phenocrysts of prismatic form with signs of sericitization both in the center and at the periphery of crystals (Figure 3B). It is zonal, with 33–45% An in the core and 15–31% An in the rim. K-feldspar occurs as porphyric crystals, rarely of microperthitic texture (albite ingrowths in orthoclase) (Figure 3). Very rarely, the grain cores are partly replaced by the secondary alteration products (pelitization), which gives them a light-brownish color. Quartz has an irregular form and occurs interstitially between the grains of salic minerals. Dark-colored minerals are dominated by biotite, which occurs in two generations (Figure 3C). The first generation is represented by idiomorphic frequently chloritized porphyric grains, and the second generation occurs as small irregular grains.

Adamellites grade into granodiorites on the peripheral part of the massif. The mineral contents are plagioclase (31–51%), K-feldspar (16–32%), quartz (25–34%), and biotite (4–16%). The texture of the rocks is hypidiomorphic granular (Figure 3D). Plagioclase occurs as prismatic crystals with a characteristic polysynthetic twinning. It is zonal with 30–40% An in the core and 10–31% An in the rim (Figure 3E). K-feldspar has irregular form and contains microperthitic segregations (Figure 3F) rich in albite component (2.1–24%). Biotite is present as tablets and flakes of irregular form.

Granites make up the central part of the massif and also form numerous dike-like bodies in adamellites of the apical zone of the massif and in sedimentary rocks beyond its limits. Their contacts with granodiorites are both gradual and sharp. The quantitative mineralogical compositions of the granites are plagioclase (30–36%), K-feldspar (30–40%), quartz (25–34%), and biotite (3–6%). They have a hypidiomorphic granular texture (Figure 3G). Plagioclase is present as prisms of irregular form, often as polysynthetic and simple twins or zonal individuals, and is partly sericitized (Figure 3H). The An content is 20–30% in the core and 4–13% in the rim. K-feldspar occurs as irregular and rectangular crystals, is weakly pelitized, and has a perthitic texture (Figure 3I). Quartz forms grains of various forms and sizes (up to 2 mm) with mosaic and wavy extinction. Biotite has isomorphous form, a characteristic pleochroism, and straight, sometimes wavy extinction.

Aplitic granites and aplites of the veined facies are widespread in both the granitoids and the enclosing sedimentary rocks. They are made of plagioclase (22–28%), K-feldspar (29–41%), quartz (36–42%), and biotite (0.1–0.7%). They have a granitic, aplitic texture (Figure 3J). Plagioclase is unzonal (5–12% An) and partly sericitized (Figure 3K). K-feldspar is perthitized and contains inclusions of plagioclase and granular quartz (Figure 3G). Quartz in the form of irregular and rounded grains is included in plagioclase and K-feldspar, and also forms small veinlets (Figure 3L). Rare inclusions of reddish-brown biotite are found in all of the rock-forming minerals.

The Sokh massif is composed of granodiorite porphyries, adamellites, granites, and aplites. Granodiorite porphyries are represented by phenocrysts of light-gray plagioclase (up to 1 cm in size) set in the fine-grained groundmass (Figure 4A). The mineral contents of the rocks are plagioclase (41–44%), K-feldspar (17–23%), quartz (25–26%), and biotite (9–13%). Plagioclase is present in two generations. The early generation is represented by porphyric prismatic crystals. Simple and polysynthetic twins (Figure 4B) and zonal individuals are observed. Most of the crystals show evidence of insignificant sericitization both in the core and at the periphery. Plagioclase of the late generation is observed in the groundmass. Cores of the crystals contain 50–55% An and the rims contain 23–45% An. K-feldspar forms xenomorphic phenocrysts in the rock matrix. The amount of albite component in it is 15.4%. Quartz forms grains of various forms and sizes (up to 2 mm). Biotite is reddish-brown in color, occurs in peripheral zones of plagioclase, and is often corroded by quartz. It is normally partly chloritized on cleavage or in the form of spots (Figure 4C).

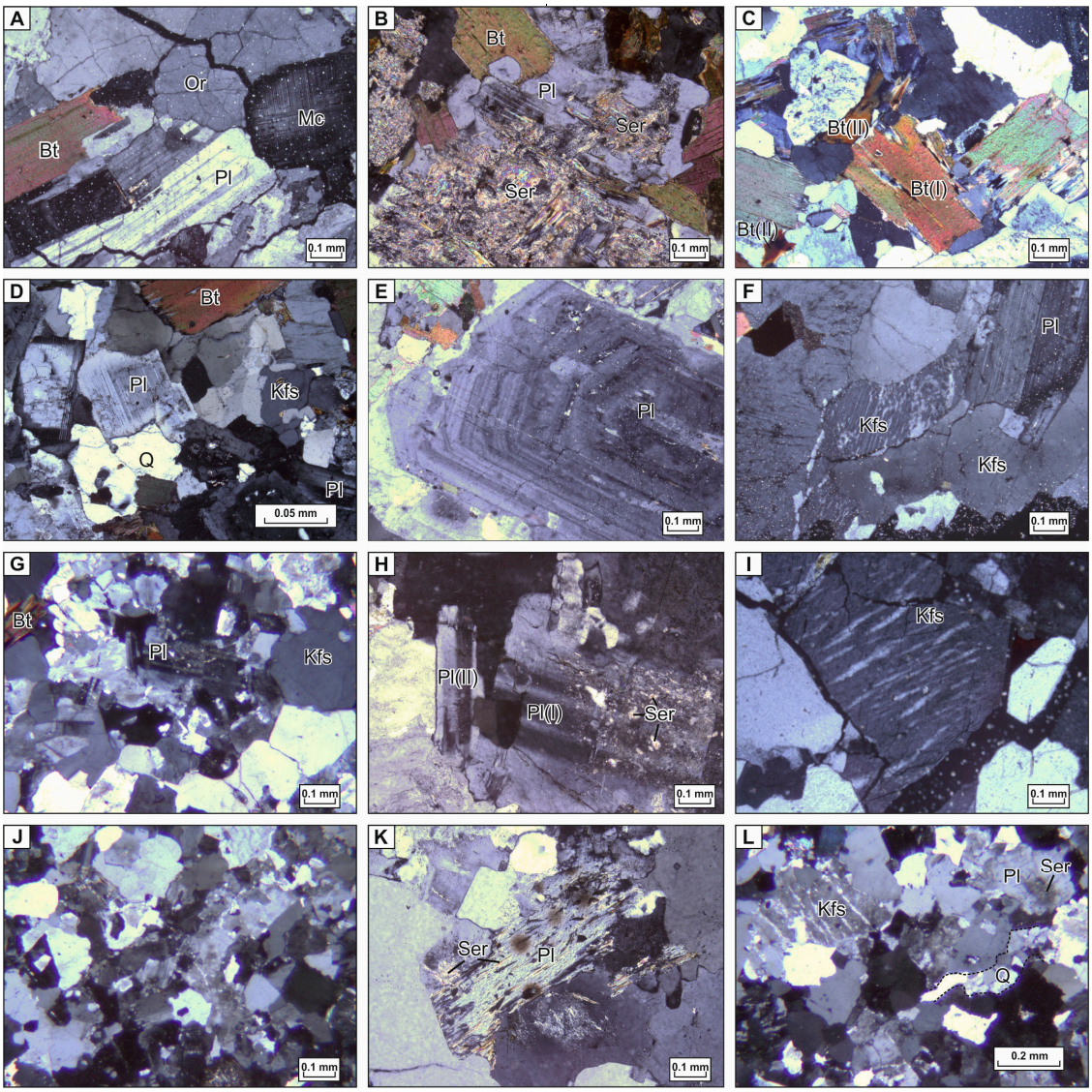

Figure 3. Photomicrographs of igneous rocks of the Ergelyakh massif, x-nicols: (**A**) hypidiomorphic granular texture of granodiorite with features of porphyric texture provided by phenocrysts of K-feldspars (Kfs) and plagioclase (sample 1184); (**B**) sericitized (Ser) plagioclase (Pl) (sample 1213); (**C**) biotite of different generations: first Bt(I), second Bt(II) (sample 1213); (**D**) general texture of adamellite (sample 1209); (**E**) zonal plagioclase (sample 1209); (**F**) microperthitic texture of K-feldspar (central part) (sample 1209); (**G**) hypidiomorphic granular texture of granite (sample 1183); (**H**) sericitized plagioclase of first-generation Pl(I), simple twins of plagioclase of second-generation Pl(II) (sample 1183); (**I**) perthitic texture of K-feldspar (center of thin section) (sample 1183); (**J**) general texture of aplite (sample 1211/2); (**K**) sericitized plagioclase Pl (sample 1211/2); (**L**) perthitized K-feldspar (upper left corner), sericite in plagioclase cores (upper right corner), quartz (Q) veinlet (dashed black line) (sample 1211/2). Or, orthoclase; Mc, microcline.

The mineral contents of adamellites are plagioclase (31–50%), K–Na–feldspar (16–30%), quartz (up to 15%), and biotite (up to 5%). The texture of the rocks is hypidiomorphic granular with porphyric elements (Figure 4D). Two generations of plagioclase are present. The first generation includes intensely sericitized porphyric prismatic crystals represented by polysynthetic and zonal individuals (Figure 4E). The An content is 20–30% in the core and 4–13% in the rim. Plagioclase of the second generation occurs in interstices between porphyric grains of K-feldspar and plagioclase. K-feldspar is also of two generations. The early generation includes irregular porphyric grains, and the later one is represented

by small grains set in the groundmass. Biotite is tabular and irregular in form. Along with quartz, it fills interstices between salic minerals of the first generation or includes K-feldspar and plagioclase of the later generation (Figure 4F).

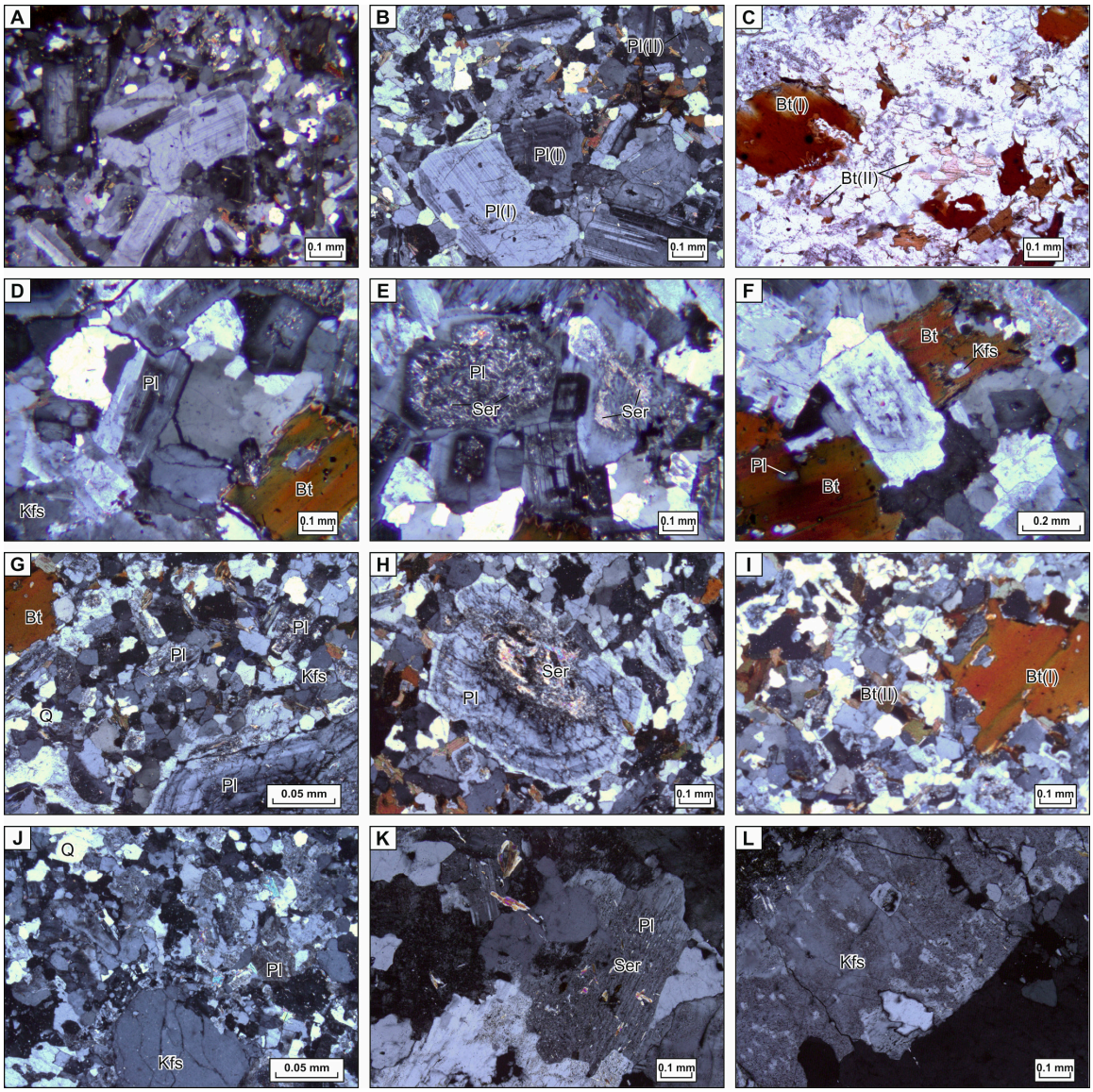

Figure 4. Photomicrographs of igneous rocks of the Sokh massif, x-nicols: (**A**) general texture of granodiorite (sample 1183); (**B**) simple twins of plagioclase of first-generation Pl(I) and second-generation Pl(II) (sample 1183); (**C**) biotite of two generations: first (Bt(I)), second (Bt(II)) (sample 1183); (**D**) general texture of adamellite (sample 1174); (**E**) sericitized plagioclase (sample 1174); (**F**) biotite with inclusions of plagioclase and K-feldspar (sample 1174); (**G**) hypidiomorphic granular texture of granite (sample 1176/1A); (**H**) zonal sericitized plagioclase (sample 1176/1A); (**I**) biotite of two generations: first (Bt(I)), second (Bt(II)) (sample 1176/1A); (**J**) general texture of aplite, porphyric grains of K-feldspar of xenogenic nature (sample 1177/8); (**K**) rare sericite in plagioclase (sample 1177/8); (**L**) perthites in K-feldspar (sample 1177/8).

The quantitative mineralogical composition of the grains is plagioclase (30–45%), K-feldspar (up to 30%), quartz (up to 20%), and biotite (up to 5%). The texture is hypidiomorphic granular and granitic (Figure 4G). Plagioclase of the first generation occurs as prisms of irregular form, and is mainly represented by fractured zonal individuals that are partly sericitized (Figure 4H). The second-generation

plagioclase is found in the groundmass in the form of simple and polysynthetic twins. An content amounts to 20–30% in the core and 4–13% in the rim. Irregular and rectangular crystals of K-feldspar are weakly pelitized. Quartz forms grains of various forms and sizes with mosaic and/or wavy extinction. Biotite occurs as isomorphous grains of two generations. The first generation includes large individuals present in interstices between porphyric grains of K-feldspar and plagioclase, and the second is represented by late-magmatic biotite in the groundmass (Figure 4I).

Aplitic granites are made of plagioclase (22–30%), K-feldspar (29–40%), quartz (up to 25%), and biotite (up to 5%). The texture of the rocks is granitic and aplitic (Figure 4J). Plagioclase is unzonal (5–12% An) and partly sericitized (Figure 4K). K-feldspar is partly perthitized and contains inclusions of plagioclase and granular quartz (Figure 4L). Quartz occurs as irregular or rounded grains. Biotite of irregular form is partly chloritized (Figure 4C,D).

3.3. Geology of the Ergelyakh Gold-Bismuth Deposit

The EIRGD occurs above the cupola of the Ergelyakh granitoid massif [6]. The granitoids and adjacent biotite hornfels are cut by en echelon lens-like, steeply dipping quartz veins up to 1 m thick and 250 m long. The main ore bodies contain a successive series of mineral associations: muscovite–tourmaline–quartz metasomatic, wolframite–tourmaline–quartz, pyrrhotite–loellingite–danaite–arsenopyrite, and bismuth–sulfotelluride [6]. Finely disseminated (0.006–0.1 mm) native gold is present in sulfoarsenides in the amount of 50–150 g/t, and free small-size gold with widely ranging fineness (750–960‰) is associated with bismuth minerals. As-bearing minerals are Co–Ni–loellingite, gersdorffite, Ni–danaite, and arsenopyrite. The late gold-bearing association of bismuth minerals includes tetradymite, A-joseite, B-joseite, and tellurobismuthite. Within the deposit and in near intrusive zones, polymetallic gold–silver mineralization has been reported [6].

Early quartz of the Ergelyakh deposit crystallized at 265–305 °C and 0.2 kbar from dilute Na and Mg chloride solutions with salinity of 4.5 wt. % to 8.6 wt. % NaCl equivalent [46]. Quartz from productive Au-bearing associations are characterized by inclusions of concentrated Na–Ca chloride solutions with salinity of 32.9–32.7 wt. % NaCl equivalent, which homogenize to liquid at temperatures of 360–255 °C, and by inclusions of Na–Mg chloride solution (3.7–6.9 wt. % NaCl equivalent) with homogenization temperatures from 360 to 190 °C and a pressure of 0.06 kbar [44]. The depth of mineralization formation is 1–2 km [1].

The intrusion-related gold–bismuth mineralization is known from polychronous compound gold deposits of the Kular-Nera slate belt [43]. It normally predates the formation of orogenic gold–quartz mineralization [9,47]. As exemplified by the Malo-Tarynskoe deposit, the orogenic Au mineralization is superposed by the intrusion-related gold–bismuth mineralization [43]. The $^{40}Ar/^{39}Ar$ age of sericite from quartz veinlets of the Malo-Tarynskoe deposit is 142.7 ± 1.4 Ma [43]. At the Malo-Tarynskoe gold–sulfide–quartz deposit, quartz–muscovite–pyrrhotite–Co–Ni– sulfoarsenide and bismuth–sulfotelluride mineral associations are identified [43]. The orogenic gold–quartz low sulfide ore bodies the Malo-Tarynskoe deposit have a sufficiently uniform mineral composition: quartz 85–95%, carbonate (ankerite) 5–15%, and ore minerals around 1–2%. The identified ore mineral assemblages are: metasomatic pyrite–arsenopyrite–sericite–quartz; veined pyrite–arsenopyrite–quartz; gold–chalcopyrite–sphalerite–galena, and carbonate–sulfosalt. Studies of stable isotopes and the fluid regime of ore formation have shown an association of the intrusion-related gold–bismuth mineralization with shallow-depth chambers of the granitoid massifs, and of orogenic gold deposits with intermediate chambers and metamorphic processes [43,44].

4. Results

4.1. Chemical Composition of Rock-Forming Minerals

The most informative rock-forming minerals of the studied massifs are K-feldspars, plagioclase, and biotite. In our study we paid special attention to them.

The data obtained show that K-feldspar in all granitoid types is characterized by wide variations in orthoclase (54.5–93.2%) and plagioclase (11.7–40.8%) components (Tables 1 and 2). Plagioclase is high in orthoclase component (2.4–8.4%) irrespective of its basicity and the type of granitoids. The content of anorthite mineral in plagioclase ranges from 42.0% to 7.6%, i.e., from andesine to albite, indicating that formation of plagioclase from the EIRGD granitoids took a long time and occurred under nonequilibrium conditions. Chemically, it contains, on average, 25–33% anorthite and 4.6–6.3% orthoclase components.

Biotites from granitoids of the EIRGD (Table 3) are mainly represented by Fe–biotite (Fe# = 0.57–0.95) except for two samples from granodiorites and one sample from adamellites of the Ergelyakh massif. The oxidation degree of Fe ($Fe^{3+}/\Sigma Fe$) in biotites of the Ergelyakh massif varies from 0.05 to 0.30, and in those of the Sokh pluton from 0.05 to 0.22. Biotite is highly ferruginous (f = 75.7–93.6%) and aluminous (K_{Al} = 0.22–0.27).

The biotite in Sokh massif is moderately ferruginous (f = 57.4–60.7%) and high in alumina (K_{Al} = 0.23). Chlorites, developed after mica, are represented by ripidolite. The degree of biotite chloritisation in granodiorites of the Ergelyakh massif is 15.0–4.7%; in adamellites, 11.4 ± 1.1%, and in granites, 9.7 ± 3.6%. For the Sokh massif, the values are 12.3 ± 0.3% in granodiorites, 10.7% in adamellites, and 9.0 ± 8.9% in granites.

Table 1. Electron microprobe analysis of K-feldspars in granodiorite from Ergelyakh massif.

Sample	SiO_2	Al_2O_3	MgO	CaO	Na_2O	K_2O	∑	Anorthite	Albite	Orthoclase
1213b14	64.63	18.09	-	-	1.83	15.00	99.55	-	15.64	84.36
1213b15	60.55	26.21	-	6.90	8.32	-	101.99	31.43	68.57	-
1213b22	63.59	21.25	-	1.72	11.63	-	98.19	7.56	92.44	-
1213b23	63.93	18.48	-	-	1.60	14.43	98.45	-	14.42	85.56
1213 b27	65.47	24.10	-	3.16	10.81	-	103.54	13.91	86.09	-
1213b28	66.13	23.49	-	2.88	11.37	-	103.87	12.28	87.72	-
1213b41	68.30	20.15	-	2.02	11.52	-	101.90	8.63	81.17	-
1213b42	66.88	18.64	0.28	-	0.72	15.17	101.69	-	6.73	93.27
1213b51	61.03	26.40	-	7.22	7.57	-	102.71	34.52	65.48	-
1213b55	65.85	20.31	-	-	4.86	10.83	101.85	-	40.86	59.45

Table 2. Chemical analysis of major and trace elements of feldspars from Ergelyakh and Sokh massifs.

Sample	Rock	Mineral	SiO_2	TiO_2	Al_2O_3	Fe_2O_3	MgO	CaO	Na_2O	K_2O	H_2O^+	P_2O_5	Σ	Li	Rb	Ba	Sr	Anorthite	Albite	Orthoclase
Ergelyakh Massif																				
1181/3a	Granodiorite	Plagioclase	61.57	0.03	24.28	0.15	0.07	5.81	6.19	1.28	0.17	0.03	99.58	3.7	24.7	370	300	31.34	60.46	8.2
		K-feldspar	69.7	0.01	17.31	0.05	0.3	1.91	3.21	7.77	0.16	0.01	100.43	6	93.2	1300	320	11.23	34.23	54.54
1022		Plagioclase	61.67	0.06	24.28	0.16	0.02	5.64	6.74	0.7	0.25	0.04	99.56	10.7	39.3	290	500	30.2	65.33	4.47
		K-feldspar	64.99	0.02	18.77	0.09	0.34	0.48	2.4	11.95	0.24	-	99.28	2.3	191	980	210	2.5	22.81	74.69
1184		Plagioclase	60.3	0.03	24.98	0.13	0.11	6.2	7.01	0.74	-	0.04	99.54	3.7	-	250	450	31.35	64.19	4.46
		K-feldspar	65.26	0.01	18.98	0.12	0.17	-	1.68	13.22	0.2	-	99.64	2.3	191	1400	240	0	16.21	83.79
1181/3b	Adamellite	Plagioclase	64.94	0.03	21.98	0.21	0.31	5.57	5.67	0.88	0.21	0.03	99.83	9.3	21	220	325	32.98	60.79	6.23
		K-feldspar	66.21	-	18.35	0.05	0.36	0.18	2.43	11.41	0.24	-	99.23	2.8	191.9	1000	150	1	24.22	74.78
1211/3		Plagioclase	69.57	0.07	18.14	0.23	0.02	3.07	5.39	0.8	-	0.1	97.39	12.5	63	180	29	22.29	70.82	6.88
		K-feldspar	64.05	0.06	17.9	0.36	0.2	0.01	1.18	13.47	-	0.13	97.36	6	323.6	-	-	0.05	11.72	88.23
1183	Granite	K-feldspar	64.82	0.04	19.1	0.13	0.31	-	2.2	12.85	0.13	0.07	99.65	8.8	750.4	1800	<200	0	20.66	79.34
1021			66.11	-	18.46	0.03	0.27	0.18	2.78	11.77	0.31	0.12	100.03	8.4	276.9	1400	69	0.95	26.17	72.88
1017	Granodiorite	K-feldspar (14.8%)	65.36	0.01	18.94	0.09	0.59	0.06	2.39	12.17	0.2	0.12	99.93	2.8	237.6	-	-	0.32	22.91	76.77
		Oligoclase (33%)	64.51	0.01	21.56	-	0.02	3.1	9.54	0.66	0.39	0.06	99.85	-	18.3	-	-	14.66	81.63	3.72
		Oligoclase (24.8%)	62.13	0.1	23.45	0.21	0.31	4.84	8.02	0.56	-	0.1	99.72	-	-	-	-	24.18	72.49	3.33
		Oligoclase (9.98%)	61.75	-	24.08	0.29	0.2	5.24	7.54	0.49	-	0.09	99.68	-	-	-	-	26.92	70.09	3
		Andesine (13.7%)	58.87	0.04	25.74	-	0.08	6.79	6.85	0.55	0.54	0.04	99.5	-	27.4	-	-	34.22	62.48	3.3
		Andesine (3.8%)	57.45	0.14	26.66	0.14	0.61	7.26	6.25	0.73	0.2	0.13	99.57	-	-	-	-	37.35	58..18	4.47
1184	Granodiorite	K-feldspar	65.26	0.01	18.98	0.12	0.17	0	1.68	13.22	0.2	-	99.64	2.3	227.6	-	-	0	16.19	83.81
		Oligoclase	64.41	0.02	21.64	-	0.02	3.79	8.77	0.76	0.25	0.03	99.69	-	18.3	-	-	18.43	77.17	4.4
			64.4	0.07	21.92	0.26	0.04	4.27	7.76	0.6	-	0.08	99.4	-	18.3	-	-	22.44	73.8	3.75
		Andesine	63.61	0.03	22.51	0.62	0.31	6.92	5.02	0.65	0.05	0.16	99.88	7.9	18.3	-	-	41.24	54.14	4.61
1181/3b	Adamellite	K-feldspar	66.21	-	18.35	0.05	0.36	0.18	2.43	11.41	0.24	-	99.23	2.8	191.9	-	-	0.99	24.21	74.8
		Andesine	62.69	0.06	23.02	0.3	0.16	6.83	6.38	0.38	-	0.09	99.91	-	-	-	-	36.28	61.32	2.4
			56.44	0.1	26.76	0.54	0.45	8.19	5.87	0.56	0.64	0.12	99.67	-	-	-	-	42.05	54.53	3.42
Sokh Massif																				
1177/5	Granodiorite	Plagioclase	66.12	0.06	21	0.19	0.01	0.01	0.1	3.93	6.54	1.22	99.18	0.23	0.09		-	22.83	68.74	8.44
		K-feldspar	65.09	0.03	18.94	0.1	0.01	0	0.35	0.15	1.57	13.06	99.3	0.2	0.17	-	-	0.8	15.3	83.9
1174	Adamellite	Plagioclase	64.84	0.03	22.16	0.13	0.01	0.01	0.01	4.63	7.01	0.71	99.54	0.12	0.05	-	-	25.5	69.85	4.66
		K-feldspar	65.14	0.01	19.06	0.08	0.01	0	0.56	0.12	2.15	11.94	99.07	0.12	0.14	-	-	0.66	21.34	78
1177/9	Aplitic granite	Plagioclase	77.9	0.06	14.32	0.42	0	0	0.09	1.78	4.56	0.53	99.66	0	0.13	-	-	16.69	77.39	5.92
1175/1		K-feldspar	66.02	0.01	18.75	0.07	0	0	0.24	0	2.44	11.6	99.13	0.23	0	-	-	0	24.22	78.78

Table 3. Chemical analysis of biotite from Ergelyakh and Sokh massifs.

	Ergelyakh Massif												Sokh Massif		
Rock	**Granodiorite**			**Adamellite**			**Granite**				**Granodiorite**		**Adamellite**	**Granite–Porphyry**	**Granite**
Mineral	**Fe–Biotite**			**Mg–Biotite**			**Fe–Biotite**						**Fe–Biotite**		
Sample	**1017**	**1022**	**1181/3a**	**1184**	**1181/3b**	**1211/3**	**1021**	**1183**	**278**	**288-g**	**1177/11**	**1177/5**	**1174**	**1177/9**	**1177**
SiO_2	33.54	35.36	34.95	35.4	35.59	34.9	34.05	34.47	34.52	35.53	35.22	34.7	34.69	32.53	34.41
TiO_2	3.18	3.74	4.12	4.25	4.13	3.61	1.3	2.03	4	3.7	4.19	4.63	3.74	2.08	4.03
Al_2O_3	18.22	16	14.41	14.02	14.14	15.02	21.07	18.86	15.71	14.31	16.44	16.82	15.01	15.42	14.83
Fe_2O_3	4.87	4.22	3.76	3.62	0.63	1.01	9.08	4.94	0.91	3.16	3.1	0.59	0.63	2.29	1.61
FeO	20.19	20.1	20	20.87	21.77	23.61	19.73	24.22	22.63	20.46	20.16	20.86	22.73	27.92	22.76
MnO	0.18	0.31	0.3	0.28	0.3	0.28	0.29	0.36	0	0.28	0.26	0.24	0.28	0.68	0.3
MgO	8.18	8.82	9.41	9.44	9.75	9.13	1.05	1.52	8.63	7.91	8.35	8.84	8.19	5.39	7.23
CaO	0.4	0.28	0.16	0.06	0.2	0.48	0.11	0.4	0.3	0.55	-	-	-	-	1.36
Na_2O	0.33	0.22	0.18	0.22	0.17	0.2	0.26	0.18	0.23	0.38	0.24	0.22	0.23	0.13	0.21
K_2O	7.69	8.37	9.13	8.73	8.52	8.48	8.2	8.92	8.41	8.76	9.09	8.68	8.6	8.17	8.42
H_2O	1.77	2.5	3.1	2.84	3.31	2.59	3.22	3.73	3.58	3.29	2.63	3.15	4.07	3.65	3.57
P_2O_5	0.12	0.14	0.02	0.06	0.06	0.08	0.08	0.06	0.52	0.18	0.06	0.06	0.06	0.06	0.16
F	0.65	0.37	0.4	0.45	0.52	0.97	0.28	0.63	1.15	1.22	0.54	0.63	1.4	0.8	0.95
Cl	0.3	0.2	0.2	0.22	0.25	0.35	0.23	0.2	-	-	0.1	0.15	0.15	0.35	0.2
O=F,Cl	0.29	0.2	0.21	0.24	0.28	0.49	0.17	0.31	-	-	-	-	-	-	-
Li_2O	0.797	0.06	0.07	0.14	0.09	0.13	0.198	0.12	0.1	0.1	0.65	0.14	0.1401	0.1603	0.1503
Rb_2O	0.068	0.06	0.06	0.05	0.067	0.057	0.091	0.09	0.05	0.06	0.07	0.085	0.0661	0.1202	0.0591
∑	99.56	100.6	100.1	100.4	99.38	100.5	99.17	100.4	100.7	99.89	101.1	99.8	99.99	99.75	100.25
Si	2.45	2.58	2.61	2.63	2.74	2.66	2.46	2.59	2.66	2.69	2.57	2.64	2.71	2.58	2.66
Al^{4+}	1.55	1.38	1.27	1.23	1.26	1.34	1.54	1.41	1.34	1.28	1.41	1.36	1.29	1.42	1.34
Al^{6+}	0.3	-	-	-	0.02	0.01	0.25	0.27	0.08	-	0	0.15	0.09	0.02	0.01
Ti	0.18	0.21	0.23	0.24	0.24	0.21	0.07	0.11	0.23	0.21	0.23	0.26	0.22	0.12	0.23
Fe^{3+}	0.54	0.43	0.29	0.25	0.07	0.12	0.99	0.56	0.11	0.36	0.32	0.07	0.07	0.27	0.19
Fe^{2+}	1.24	1.23	1.25	1.29	1.4	1.51	1.19	1.52	1.46	1.3	1.23	1.33	1.49	1.85	1.47
Mn	0.01	0.02	0.02	0.02	0.02	0.02	0.02	0.02	-	0.02	0.02	0.02	0.02	0.05	0.02
Mg	0.89	0.96	1.05	1.04	112	1.04	0.11	0.17	0.99	0.89	0.91	1	0.95	0.64	0.03
Li	-	-	-	-	-	-	-	-	-	-	0.19	0.04	0.04	0.05	0.05
Ca	0.03	0.02	0.01	-	0.02	0.04	0.01	0.03	0.02	0.04	0	0	0	0	0.11
Na	0.05	0.03	0.03	0.03	0.03	0.03	0.04	0.03	0.03	0.06	0.03	0.03	0.03	0.02	0.03
K	0.72	0.78	0.87	0.83	0.84	0.82	0.75	0.86	0.83	0.85	0.84	0.84	0.86	0.83	0.83
OH	1.84	1.89	1.89	1.87	1.84	1.72	1.91	1.82	1.72	1.71	1.86	1.83	1.63	1.75	1.74
F	0.15	0.09	0.09	0.11	0.13	0.23	0.06	0.15	0.28	0.29	0.12	0.15	0.35	0.2	0.23
Cl	0.01	0.02	0.03	0.03	0.03	0.05	0.03	0.03	-	-	0.01	0.02	0.02	0.05	0.03
Mg#	0.33	0.36	0.39	0.38	0.43	0.39	0.05	0.08	0.39	0.35	0.37	0.42	0.38	0.23	0.33
Fe^2/SFe	0.7	0.73	0.75	0.76	0.95	0.93	0.55	0.73	0.93	0.78	0.78	0.95	0.95	0.87	0.89
Al/(Al + Si)	0.64	0.53	0.49	0.47	0.47	0.51	0.73	0.64	0.54	0.47	0.55	0.57	0.51	0.56	0.51

4.2. Chemical Composition of Accessory Minerals

The principal accessory minerals of granitoids from the Ergelyakh and Sokh massifs are ilmenite, zircon, and apatite. Grains of orthite, anatase, fluorite, monazite, rutile, garnet, and sulfides (arsenopyrite, loellingite, pyrrhotite, pyrite, bismuth minerals, galena) are rare to solitary [6].

Garnets from granitoids of both massifs are represented by almandine with varying amounts of spessartine, pyrope, andradite, grossular, and majorite. In the Ergelyakh massif, the quantity of almandine component in garnets (Table 4) increases from granodiorites (76.2–80.9%) to granites (82.2–83.3%). The amount of andradite component also grows from 1.3–2.0% in granodiorites to 1.2–3.4% in granites. Most pronounced are changes in pyrope and spessartine components. The content of spessartine in garnets from granodiorites is 4.2–6.2%, and in garnets from granites is up to 9.6–11.2%. Pyrope in garnets sharply decreases from granodiorites (10.12–13.65%) to granites (2.01–3.0%). This is accompanied by decreasing Mg content (Mg#) of garnets from granodiorites (0.14–0.15) to granites (0.03–0.04) and by an increasing degree of iron oxidation ($Fe^{3+}/\Sigma Fe$) from 1.6–1.9 to 3.6–4.2, respectively.

Garnets from the Sokh massif do not exhibit a distinct trend in composition. The amount of almandine in garnets from granitoids (Table 4) varies within a narrow range (69.7–78.2%). Garnets from adamellites are somewhat higher in almandine (70.8–78.2%) and those from granodiorites and aplitic granites have lower almandine content: 71.7–72.9% and 69.7–71.8%, respectively. A more pronounced trend is observed for spessartine in garnets, which is high in granodiorite porphyries and aplitic granites (24.6–25.6%) and low in adamellites (1.7–5.5%). Garnets from adamellites are also marked by elevated pyrope mineral content (13.5–22.0%), which is much higher than in granodiorites and aplitic granites (0.4%). This promotes differences in Mg# value, which is higher in garnets from adamellites (0.02–0.23) than from granodiorites and aplitic granites (0.03–0.14). Garnets from adamellites also exhibit a higher degree of iron oxidation ($Fe^{3+}/\Sigma Fe$ = 1.2–2.6) as compared to granodiorites and aplitic granites, which is zero. These differences in the composition of garnets are due to different conditions of their formation.

Table 4. Chemical analysis of garnets from Ergelyakh and Sokh massifs.

	Ergelyakh Massif													Sokh Massif						
Rock	**Granodiorite**					**Granite**			**Granodiorite**					**Adamellite**			**Aplitic Granite**			
Sample	**1181/3a**			**1181/34**		**1021**			**1177/11**					**1177/5**			**1177/7**			
	1	**2**	**3**	**1**	**2**	**1**	**2**	**3**	**1**	**2**	**3**	**4**	**5**	**1**	**2**	**3**	**1**	**2**	**3**	**4**
SiO_2	32.7	37.7	37.8	37.7	37.8	36.7	36.6	36.8	38.2	37.8	37.7	38.3	36.7	36.4	36.2	36.7	37.3	37.4	37.0	37.4
TiO_2	0.13	0.16	0.02	0.16	-	-	0.01	0.03	0	0.14	0.16	0.01	0.14	0	0.05	0.02	0	0.09	0.02	0
Al_2O_3	20.1	20.0	20.2	20.0	20.2	20.3	20.1	20.2	20.9	20.6	20.4	21.0	20.6	20.0	19.9	20.4	20.3	20.1	20.5	20.2
Fe_2O_3	-	1.47	1.61	-	-	-	-	-	0	1	0	0	1.06	0	0	0	0	0	0	0
FeO	35.8	33.5	35.4	34.8	36.8	38.6	38.9	38.3	33.2	35.6	35.7	32.7	35.6	31.2	31.4	31.4	31.1	31.27	30.6	31.4
MnO	2.3	2.8	1.9	2.8	1.9	4.7	4.9	4.2	2.3	0.7	2.4	2.2	0.7	10.6	10.5	10.6	10.9	10.8	11.1	10.7
MgO	3.5	3.5	3.5	3.5	3.5	0.6	0.5	0.8	5.7	4.2	3.5	5.7	4.2	0.5	0.5	0.5	1.0	1.1	0.9	1.1
CaO	1.1	1.5	0.7	1.5	0.7	0.8	0.5	1.2	0.8	1.2	1.3	0.8	1.3	0.3	0.4	0.3	0.4	0.4	0.4	0.4
Cr_2O_3	-	0.21	-	-	-	-	0.02	-	-	-	-	0.06	-	-	0.01	0.01	-	0.02	-	-
Σ	101.8	100.7	100.8	100.5	100.8	101.7	101.5	101.4	101.1	101.2	101.2	100.7	100.2	98.9	98.9	99.8	101.0	101.2	100.5	101.2
Fe^{2+}	2.34	2.29	2.43	2.29	2.43	2.52	2.54	2.51	2.12	2.36	2.32	2.12	2.35	2.17	2.19	2.16	2.12	2.12	2.09	2.13
Mn	0.15	0.19	0.13	0.19	0.13	0.32	0.33	0.29	0.15	0.05	0.16	0.15	0.05	0.75	0.74	0.74	0.75	0.74	0.77	0.74
Mg	0.41	0.40	0.39	0.39	0.39	0.07	0.06	0.10	0.67	0.49	0.42	0.66	0.50	0.05	0.04	0.06	0.10	0.10	0.11	0.10
Ca	0.10	0.13	0.06	0.13	0.06	0.07	0.04	0.10	0.07	0.10	0.11	0.07	0.11	0.03	0.03	0.02	0.04	0.04	0.04	0.04
$\Sigma_{dodecahedron}$	2.99	3.00	3.00	3.00	3.00	2.98	2.98	3.00	3.00	3.00	3.00	3.00	3.00	3.00	3.00	2.99	3.00	3.00	3.00	3.00
Si	-	0.019	0.027	0.024	0.027	-	-	-	0.002	-	0.004	0.011	-	0.036	0.019	0.027	0.032	0.036	0.023	0.035
Ti	0.008	0.096	0.001	0.010	-	-	0.001	0.002	-	0.008	0.010	0.001	0.008	-	0.003	0.001	-	0.006	0.001	0
Al	1.96	1.89	1.90	1.89	1.90	1.92	1.91	1.92	1.94	1.92	1.92	1.95	1.89	1.96	1.96	1.99	1.94	1.93	1.98	1.93
Cr	-	0.0133	-	-	-	-	0.0013	-	-	-	-	0.0037	-	-	0.0007	0.0007	0	0.0013	-	0
Fe^{2+}	-	0.0096	0.0012	0.0097	-	-	-	-	-	0.004	0.0096	0.0006	0.039	-	0.0012	-	-	-	-	0
Fe^{3+}	0.036	0.038	0.041	0.038	0.042	0.102	0.108	0.091	0.062	0.063	0.056	0.025	0.064	-	-	-	-	-	-	0.002
Mg	-	0.019	0.027	0.024	0.027	-	-	-	0.002	-	0.004	0.011	-	0.004	0.019	-	0.242	-	0.0008	0.035
$\Sigma_{octahedron}$	2.01	2.09	2	2	2	2.01	2.01	2.00	2	2	2	2	2	2	2	2.0143	2	2	2	2
Si	2.99	3	3	3	3	2.98	2.98	2.99	3	3.00	3	3	2.94	3	3	3	3	3	3	3

Table 4. *Cont.*

	Ergelyakh Massif													Sokh Massif						
Rock	**Granodiorite**					**Granite**			**Granodiorite**					**Adamellite**			**Aplitic Granite**			
Sample	**1181/3a**			**1181/34**		**1021**			**1177/11**					**1177/5**			**1177/7**			
	1	**2**	**3**	**1**	**2**	**1**	**2**	**3**	**1**	**2**	**3**	**4**	**5**	**1**	**2**	**3**	**1**	**2**	**3**	**4**
Al	0.04	-	-	-	-	0.02	0.02	0.02	-	0.00	-	-	0.06	-	-	-	-	-	-	-
$\Sigma_{tetrahedron}$	3	3	3	3	3	3	3	3	3	3	3	3	3	3	3	3	3	3	3	3
$Fe^{3+}/\sum Fe$	1.6	1.7	1.9	1.6	1.7	4.0	4.2	3.6	2.8	2.6	2.3	1.2	2.6	0	0	0	0	0	0	0.08
Mg#	-	-	-	-	-	-	-	-	0.24	0.17	0.15	0.02	0.17	0.03	0.03	0.03	0.14	0.04	0.05	0.06
Spess	5.1	6.2	4.2	6.2	4.2	10.7	11.2	9.6	5.1	1.7	5.5	4.9	1.7	24.9	24.7	24.7	24.9	24.6	25.6	24.6
Pyr	13.7	11.3	10.2	10.7	10.1	2.3	2.1	3.0	22.0	16.4	13.5	21.0	16.5	1.4	0	1.9	0.9	0.8	3.5	0
Alm	77.8	76.2	80.8	76.3	80.9	83.0	82.2	83.3	69.7	78.2	77.0	70.8	76.2	71.7	72.9	72.2	70.5	71.8	69.7	71.0
Gros	1.5	0.9	-	1.5	-	-	-	-	-	0	-	0.7	-	-	0.3	0.6	0.9	0.1	0.0	0.8
Andr	1.3	1.9	1.9	1.9	2.0	2.4	1.2	3.4	2.2	2.8	2.6	1.1	3.2	-	0	0	-	0	-	-
Skageti	-	-	-	-	0.1	-	-	0.3	0.8	0.3	-	-	0.01	-	-	-	-	-	-	-
Maigorit	-	1.9	2.7	2.4	2.7	-	-	-	-	-	0.4	1.1	-	0.4	1.4	-	2.4	2.5	-	3.2
Shorlomit	0.4	-	-	-	-	-	0.0	0.1	-	0.2	-	-	0.4	-	-	-	-	-	-	-
Morimotoit	-	1.0	0.1	1.0	-	-	-	-	-	0.4	1.0	0.1	-	-	0.3	-	-	0.6	0.1	-
Uvarovite	-	0.7	-	-	-	-	0.1	-	-	-	-	0.2	-	-	0.0	0.0	0.0	0.1	-	-

4.3. Petro- and Geochemical Composition of Granitoids of Ergelyakh and Sokh Massifs

Granitoids of both massifs belong to the alkaline series due to their high-K variety (Table 5). They contain moderate amounts of alumina (ASI for the Ergelyakh massif is 1.0–1.2 and for the Sokh massif is 1.0–1.1). In terms of petrographic and petrochemical data, the rocks of both massifs correspond to the granodiorite–granite complex. They have similar petrochemical composition (Table 5) but differ in the number of alkaline elements. Granodiorite porphyries and adamellites of the Sokh massif characteristically have a higher $K_2O + Na_2O$ sum (7.9 ± 0.4% and 7.9 ± 0.2%, respectively) in contrast to the same rocks from the Ergelyakh massif (6.6 ± 0.6% and 7.0 ± 1.0%) (Figure 5A). They are rather close in Na_2O content (3.9 ± 0.1 and 3.8 ± 0.2 in the Sokh and 3.6 ± 0.3 and 3.5 ± 0.6 in the Ergelyakh, respectively) but differ drastically in K_2O quantity (Figure 5B,C). In granodiorite porphyries and adamellites of the Sokh massif, K_2O content is equal to 4.0 ± 0.02% and 4.1 ± 0.3%, respectively, while in the same rocks of the Ergelyakh pluton it is 2.9 ± 0.3% and 3.4 ± 1.0%. Accordingly, they differ in K_2O/Na_2O value, which is higher for granodiorites and adamellites of the Sokh massif (1.05 ± 0.03 and 1.1 ± 0.14, respectively) than for analogous rocks of the Ergelyakh massif (0.81 ± 0.08 and 0.99 ± 0.33). Na content slightly decreases in the granodiorite–adamellite–granite–aplite series of the Ergelyakh (2.7 ± 0.26%, 2.62 ± 0.3%, 2.58 ± 0.1%, 2.48 ± 0.21%) and Sokh (2.88 ± 0.07%, 2.8 ± 0.17%, 2.82 ± 0.37%, 2.51 ± 0.21%) massifs. K content exhibits a more pronounced tendency to increase: 2.42 ± 0.28%, 2.84 ± 1.0%, 3.83 ± 0.3%, 4.12 ± 0.32% for granitoids of the Ergelyakh massif and 3.32 ± 0.03%, 3.42 ± 0.4%, 3.47 ± 0.29%, 4.66 ± 0.61% for rocks of the Sokh massif. The K/Na value, accordingly, increases from granodiorites through granites to aplites. This is particularly evident for the Ergelyakh massif granitoids. In granodiorites this value is 0.9 ± 0.1; in adamellites, 1.1 ± 0.41; in granites, 1.5 ± 0.19; and in aplites, 1.68 ± 0.27. The K/Na ratio in the Sokh massif granodiorites (1.16 ± 0.04), adamellites (1.23 ± 0.22), and granites (1.24 ± 0.11) also follows this tendency, with a sharp increase observed in aplites (1.82 ± 0.32).

A higher content of spessartine mineral and a lower amount of pyrope component may indicate relatively low pressures during the rock emplacement [48].

Granitoids of the early phases of both massifs differ in Li and Rb contents (Table 5). In granodiorites and adamellites of the Ergelyakh massif, the Li content is 52.8 ± 7.2 and 45.01 ± 5.3 ppm, and in analogous rocks of the Sokh massif it is 85 ± 2.9 and 73.5 ± 2.1 ppm, respectively. In granites and aplites of both massifs, the Li content is nearly identical: 46.9 ± 22.5 and 18.5 ± 11.0 ppm in the Ergelyakh massif and 45.3 ± 8.0 and 18.6 ± 5.6 ppm in the Sokh massif, respectively (Figure 5D). In general, there is a tendency for decreased Li content from early to late phases of the two massifs. No regularity is observed in Rb distribution in granitoids of different phases of the massifs. Its content is somewhat higher in the Sokh massif rocks. Granodiorites and adamellites of the Ergelyakh massif contain 108.3 ± 18.3 and 101.4 ± 37.1 ppm Rb, respectively, and analogous rocks of the Sokh pluton contain 132 ± 20 and 147.6 ± 18.7 ppm Rb. However, average Rb content in the granites of the Ergelyakh massif (158.2 ± 21) is higher than in those of the Sokh massif (125.3 ± 7.5). In aplites from these massifs, Rb content is rather close (117.9 ± 21 and 125.6 ± 7.5 ppm, respectively). The K/Rb value for granitoids of the Ergelyakh massif increases from granodiorites (227 ± 27) through adamellites (277 ± 84) and granites (244 ± 17) to aplites (362 ± 89). A similar tendency for K/Rb variation is characteristic of the Sokh massif granitoids: granodiorites (254 ± 36) and adamellites (232 ± 2) have low K/Rb ratios, while granites (277 ± 11) and aplites (372 ± 51) exhibit higher values. On the K/Rb–Rb diagram (Figure 6), granitoids of the studied massifs do not follow a general trend typical of granitoids differentiated from a single magma chamber, but rather form a series of individual fractionation trends for the rocks of different phases in the massif emplacement. The K/Rb ratio increases from granitoids of the early to late phases, which corresponds to anatectic granites [49].

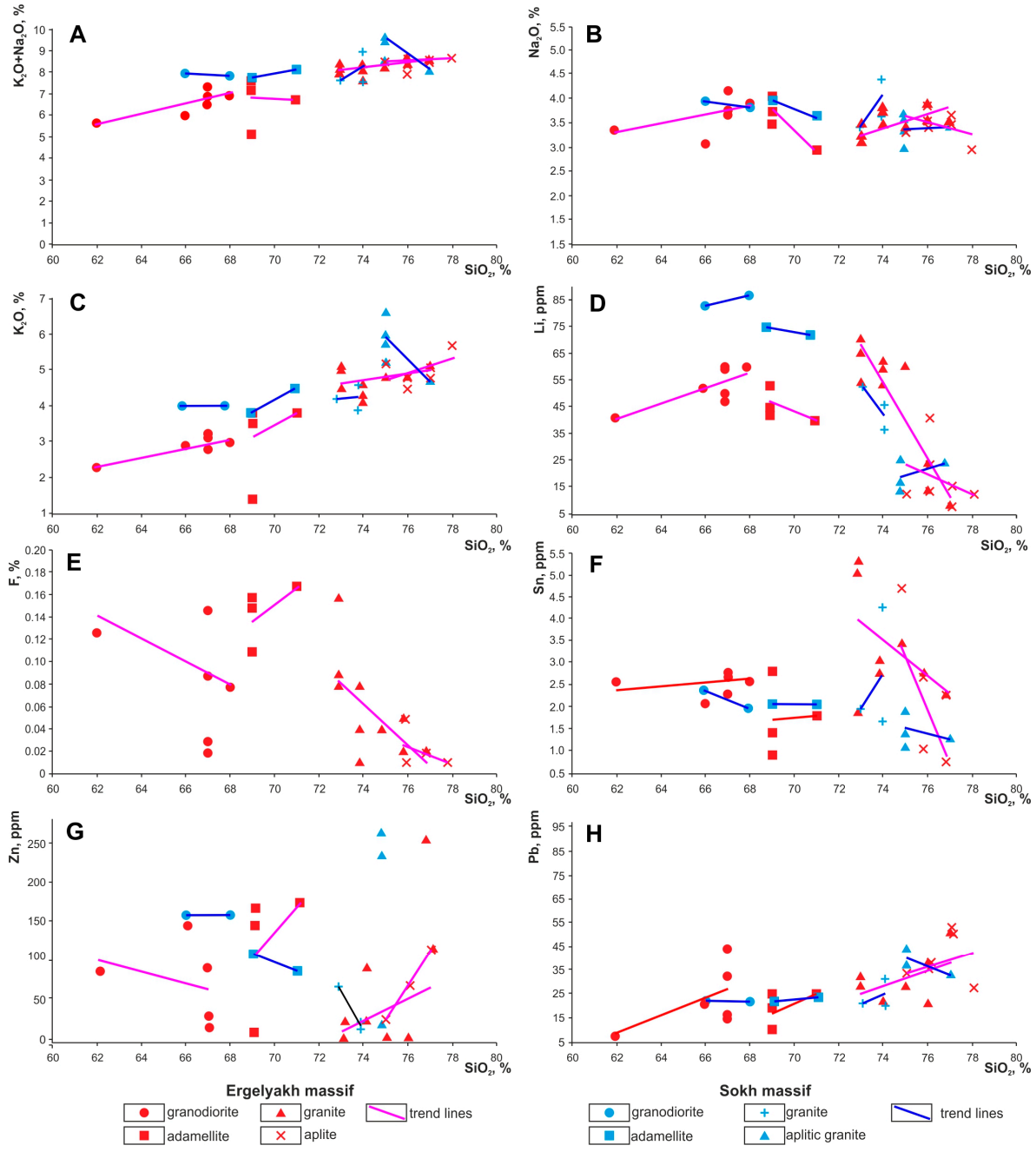

Figure 5. Variation diagrams for granitoids of Ergelyakh and Sokh massifs: (**A**) $K_2O + Na_2O–SiO_2$; (**B**) $Na_2O–SiO_2$; (**C**) $K_2O–SiO_2$; (**D**) F–SiO_2; (**E**) Li–SiO_2; (**F**) Sn–SiO_2; (**G**) Zn–SiO_2; (**H**) Pb–SiO_2.

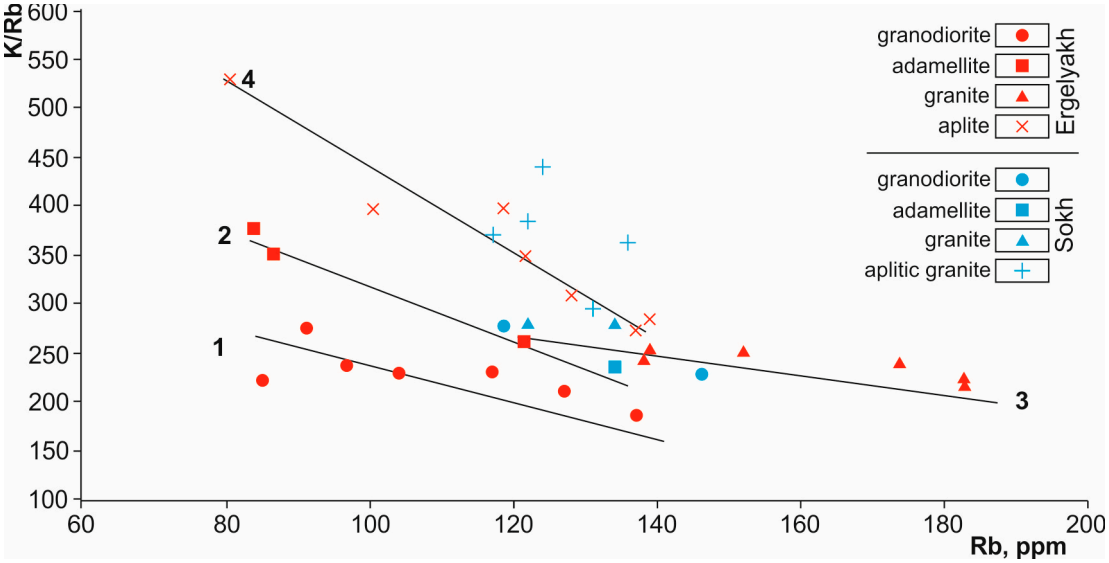

Figure 6. Rb–K/Rb diagram for granitoids of Ergelyakh and Sokh massifs. 1–4—trend lines for granitoids: 1—granodiorite, 2—adamellites, 3—granites, 4—aplites and aplitic granites.

Granitoids of the Ergelyakh massif have a generally close Sr content (granodiorites, 259 ± 53 ppm; adamellites, 238 ± 136 ppm; granites, 244 ± 17 ppm), with a sharply decreased aplite content (74 ± 51 ppm). In the Sokh massif, Sr content in granodiorites is 235 ± 21 ppm, close to that in analogous rocks of the Ergelyakh pluton, but decreases from adamellites (180 ± 21 ppm) through granites (117 ± 50 ppm) to aplites (58 ± 33 ppm). The Rb/Sr ratio varies in different phases of the massifs depending on the distribution of these elements in the rocks. A tendency is observed for an increase in this value from granodiorites to aplites: 0.41 ± 0.1 and 0.57 ± 0.14 in granodiorites, 0.55 ± 0.31 and 0.84 ± 0.24 in adamellites, 2.43 ± 1.38 and 1.28 ± 0.77 in granites, and 2.51 ± 1.85 and 2.87 ± 1.55 in aplites of the Ergelyakh and Sokh massifs, respectively.

Ba from the Sokh massif granitoids follows the same trend as Sr (Table 5). The maximum concentration is found in granodiorites (545 ± 120 ppm), with lower amounts observed in adamellites (395 ± 64 ppm), granites (347 ± 102 ppm), and aplites (300 ± 147 ppm). The Ergelyakh massif granitoids do not show regular changes in Ba content between rocks of different phases. The maximum quantity of the element is recorded in granites (637 ± 349 ppm), with lower values found in granodiorites and adamellites (507 ± 92 and 468 ± 39 ppm, respectively). Aplites contain the lowest amount of Ba (434 ± 432 ppm).

F behavior is nearly similar in the rocks of the two massifs, but the Sokh massif granitoids are markedly richer in F (Table 5, Figure 5E). The highest F concentrations are found in adamellites (0.15 ± 0.03% in the Ergelyakh and 0.26 ± 0.08% in the Sokh massif). Granodiorites of the Ergelyakh and Sokh massifs contain 0.1 ± 0.07% and 0.17 ± 0.04%; granites, 0.05 ± 0.04% and 0.09 ± 0.07%; and aplites 0.01 ± 0.02% and 0.05 ± 0.02% F, respectively. A similar tendency is observed for biotites of the Ergelyakh massif. Biotites from granodiorites of the Ergelyakh massif contain 0.47 ± 0.13%; from adamellites, 0.75 ± 0.32%; and from granites, 0.8–0.5% F. Biotites of the Sokh massif are somewhat richer in F as compared to the Ergelyakh massif (0.59 ± 0.06% from granodiorites and 0.88 ± 0.11% from granites).

The distribution of the discussed elements in granitoids is controlled by the mineral content of the rocks and the amounts of these elements in the minerals. Particularly, K-feldspar and biotite are the main carriers of Rb in the rocks. K-feldspars and biotites from granodiorites of the Ergelyakh massif contain 199 ± 58 and 544 ± 68 ppm Rb, respectively. In adamellites, these minerals are richer in Rb (258 ± 93 and 568 ± 65 ppm). The highest Rb values are found in K-feldspar and biotite from granites (514 ± 334 and 665 ± 191 ppm). Sr in the EIRGD granitoids is mainly concentrated in feldspars.

K-feldspars from the Ergelyakh massif granodiorites contain 257 ± 57 ppm Sr; from adamellites, 150 ppm; and from granites, 134 ± 93 ppm. Plagioclase from granodiorites is high in Sr (417 ± 104 ppm) and that from adamellites contains 177 ± 209 ppm Sr. K/Rb ratios in K-feldspars and plagioclases of the massif show a similar trend. K-feldspars from granodiorites have the highest K/Rb ratio (538 ± 102).

The value is decreased in adamellites (419 ± 105) and is the lowest in granites (247 ± 149). Plagioclases from Ergelyakh massif granodiorites have a K/Rb value of 278 ± 98, and those from adamellites have a value of 227 ± 171. K/Rb ratios of K-feldspars from the Sokh massif decrease from granodiorites (423) through adamellites (390) to aplites (350). Rb/Sr values in K-feldspars of the Ergelyakh massif increase from granodiorites (0.67 ± 0.33) through adamellites (1.28) to granites (4.09 ± 0.11).

Ore elements are unevenly and irregularly distributed in granodiorites of both massifs (Table 5). In the Ergelyakh massif, high V and Co concentrations (46.8 ± 15.2 and 42.0 ± 23.5, and 7.8 ± 2.3 and 8.9 ± 2.3 ppm, respectively) are found in granodiorites and adamellites, with lower contents recorded in granites and aplites (10.8 ± 7.4 and 8.1 ± 6.1, and 2.4 ± 1.5 and 2.3 ± 1.4 ppm). Granodiorites and adamellites of the Sokh massif are also characterized by large amounts of V and Co (45.5 ± 0.7 and 21 ± 1.4, and 8.2 ± 0.6 and 5.1 ± 1.1 ppm, respectively), while granites and aplites contain smaller amounts of these elements (10.5 ± 7.8 and 4.0 ± 2.3, and 4.2 ± 1.5 and 2.4 ± 0.4 ppm, respectively). Ni is irregularly distributed in the rocks of the massifs and varies within a narrow range. Maximum concentrations are observed in granodiorites of the Sokh and adamellites of the Ergelyakh massif (19.5 ± 0.7 and 18.3 ± 7.9 ppm, respectively), and minimum values in granites of the Ergelyakh massif (9.9 ± 6.1 ppm) and granites and aplites of the Sokh pluton (11.0 ± 2.1 and 9.2 ± 2.9 ppm, respectively). Granodiorites and aplites of the Ergelyakh pluton have similar Ni content (15.5 ± 6.1 and 14.0 ± 9.8 ppm, respectively). Cu is evenly distributed in the Ergelyakh massif rocks: 11.6 ± 2.5 ppm in granodiorites, 12.0 ± 1.3 ppm in adamellites, 10.4 ± 1.1 ppm in aplites, and 7.2 ± 3.2 ppm in granites. In the Sokh massif, Cu distribution is less even. Maximum concentration of the element is registered in aplites (25.3 ± 37.3 ppm). Granodiorites and granites contain less Cu (13.8 ± 1.1 ppm and 8.0 ± 1.2 ppm, respectively). Minimum Cu content is found in adamellites (2.6 ± 3.7 ppm).

Sn content is low in both massifs, but is somewhat higher in the Ergelyakh granitoids (1.7 ± 0.8 to 3.4 ± 1.3 ppm) than in rocks of the Sokh massif (1.4 ± 0.3 to 2.7 ± 1.4 ppm) (Table 5, Figure 5F). Zn distribution in the rocks of the massifs is uneven and irregular. The highest Zn content is observed in granodiorites of the Sokh massif (170 ppm) and the lowest in granites of both the Ergelyakh (47.2 ± 44.5 ppm) and Sokh (45.3 ± 29.4 ppm) massifs. In the Ergelyakh massif, the highest Zn values are found in adamellites (128.8 ± 73.3 ppm) (Figure 5G). Granodiorites and aplites contain 81.2 ± 49.0 and 78.7 ± 41 ppm Zn, respectively. In the Sokh pluton, close Zn amounts are noted in adamellites (109.5 ± 14.8 ppm) and aplites (114.2 ± 129.6 ppm). Pb content is almost identical in granodiorites (22.6 ± 13.6 ppm) and adamellites (19.8 ± 7.1 ppm) of the Ergelyakh massif and in granodiorites (22.0 ppm), adamellites (23.0 ± 1.4 ppm), and granites (25.0 ± 6.1 ppm) of the Sokh pluton (Figure 5H). Granites and aplites have relatively large amounts of this element (30.4 ± 9.5 ppm and 37.3 ± 11.5 ppm, respectively). The highest Pb value (49.4 ± 26.4 ppm) is found in adamellites (128.8 ± 73.3 ppm). Granodiorites and aplites contain 81.2 ± 49.0 and 78.7 ± 41 ppm Zn, respectively. In the Sokh pluton, close Zn amounts are noted in adamellites (109.5 ± 14.8 ppm) and aplites (114.2 ± 129.6 ppm). Pb content is almost identical in granodiorites (22.6 ± 13.6 ppm) and adamellites (19.8 ± 7.1 ppm) of the Ergelyakh massif and in granodiorites (22.0 ppm), adamellites (23.0 ± 1.4 ppm), and granites (25.0 ± 6.1 ppm) of the Sokh pluton. Granites and aplites have relatively large amounts of this element (30.4 ± 9.5 ppm and 37.3 ± 11.5 ppm, respectively). The highest Pb value (49.4 ± 26.4 ppm) is found in aplites of the Sokh massif.

Table 5. Chemical analysis of Ergelyakh and Sokh massif granitoids.

Sample	Rock	SiO_2	TiO_2	Al_2O_3	Fe_2O_3	FeO	MnO	MgO	CaO	Na_2O	K_2O	H_2O^+	P_2O_5	S	Cl	F	∑	Li	Rb	Sr	Ba	V	Co	Ni	Cu	Zn	Sn	Pb	Y	Nb	Zr	Hf	Ta
Ergelyakh Massif																																	
1181/3a	Granodiorite	66	0.8	16.1	-	4.8	0.06	1.53	3.6	3.04	2.9	0.61	0.2	0.09	-	0.21	100.2	52	104	260	500	49	9	19	13	149	2.1	21	23	12	139	4	1.2
1017		67	0.8	15.8	1.2	3.1	0.01	1.38	2.4	4.12	3.2	0.85	0.2	0.02	0.1	0.03	100.2	59	127	360	400	33	7	12	8.7	27	2.8	33	23	13	160	-	-
1022		67	0.6	15.1	-	4	0.01	2.05	3.1	3.7	2.8	1.15	0.2	0.02	0.1	0.02	99.76	50	97	213	493	-	4	6	13	40	7.2	44	-	-	180	-	-
1184		67	0.6	15.7	0.11	4	0.06	1.22	3.1	3.64	3.2	0.8	0.2	0.02	-	0.15	100.2	47	117	240	450	32	8	15	-	96	2.3	15	30	13	190	5	-
1016		68	0.6	15.4	0.31	3.9	0.06	1.16	3	3.88	3	0.67	0.2	-	-	0.08	100.1	60	91	220	670	51	10	17	-	-	2.6	-	-	-	140	-	-
1015		67	0.7	15.2	0.71	4.2	0.07	1.22	2.8	3.74	3.1	-	0.2	-	-	0.09	99.18	60	137	-	-	-	-	-	-	-	2.7	16	-	-	-	-	-
1212		62	0.8	16.8	0.87	4	0.09	2.3	4.2	3.33	2.3	1.41	0.2	0.07	-	0.13	98.49	41	85	260	530	69	10	24	-	94	2.6	7	-	-	-	-	-
1178/4	Adamellite	69	0.4	15	-	3.1	0.03	0.92	2.3	4.01	3.6	0.67	0.1	0.01	-	0.16	99.23	42	87	190	510	30	7	13	-	170	1.4	25	-	-	-	3	1.3
1210		69	0.5	14.8	0.34	3.5	0.05	1.21	2.4	3.44	3.8	1.03	0.2	-	-	0.11	100.5	53	122	200	490	34	8	14	-	150	2.8	19	-	-	200	-	-
1181/3b		71	0.5	14.2	0.26	2.2	0.03	0.74	2.4	2.91	3.8	1.07	0.1	0.07	-	0.17	99.74	40	84	160	440	27	5	16	11	175	1.8	25	32	9	91	-	-
1019		69	0.8	15.6	-	3.1	0.02	1.47	4.1	3.7	1.4	-	0.2	-	-	0.15	99.51	45	69	480	430	77	16	30	13	20	0.9	10	-	-	-	-	-
1211/3	Granite	73	0.2	14.2	0.12	2.4	0.03	0.57	1.5	3.45	4.5	0.19	0.1	-	-	0.16	100.5	54	139	120	510	21	5	13	-	35	1.9	32	-	-	-	-	-
1021		74	0.1	12.9	2.25	1.6	0.01	0.35	0.4	3.45	4.1	0.76	0.1	-	-	0.01	99.72	59	138	30	670	-	-	-	-	-	-	-	-	-	-	-	-
1182		74	0.1	13	-	2.1	0.02	0.09	0.5	3.78	4.3	0.97	0.1	-	-	0.08	98.95	53	139	37	710	5	2	12	7	100	2.8	22	31	10	57	2	0.9
1213/1		74	0.1	13.4	-	1.8	0.03	0.1	0.5	3.73	4.6	0.51	0.1	-	-	0.04	98.87	62	152	49	640	3	2	6	4	37	3.1	22	3	-	-	-	-
1211/2		76	0	12.6	-	1.5	0.01	0.1	0.4	3.53	4.8	0.69	0.1	0.02	-	0.05	99.38	24	139	16	89	3	5	2	12	11	2.8	38	17	6	39	2	1.9
1016/3		76	0.1	12.8	0.31	0.6	0.01	-	0.6	3.85	4.8	0.64	-	-	-	0.02	100	14	101	140	1300	9	2	19	-	-	-	21	-	-	-	-	-
1211		77	0.1	12.6	-	1.1	0.01	0.06	0.4	3.47	5.1	0.34	0.1	0.01	-	0.02	99.92	8.4	80	19	130	5	3	8	-	120	2.3	51	-	-	-	-	-
1020/1		73	0.2	14	0.39	1.7	0.03	0.25	0.6	3.22	5.1	-	0.2	-	-	0.08	99.04	65	174	130	650	19	2	21	10	-	5.1	28	-	-	-	-	-
1020/4		73	0.2	14	0.53	1.6	0.04	0.21	0.5	3.09	5	-	0.2	-	-	0.09	98.89	70	183	120	840	15	2	13	6	14	5.4	32	-	-	-	-	-
1020/3		75	0.2	13.5	0.65	1.4	0.04	0.11	0.5	3.36	4.8	-	0.1	-	-	0.04	99.54	60	183	120	830	18	2	12	4.3	13	3.5	28	-	-	-	-	-
1017/1	Aplite	75	-	12.2	0.13	0.5	0	1.79	0.4	3.29	5.2	0.28	-	0.02	-	-	98.83	13	122	-	528		5	5	11	38	4.8	34	-	-	-		-
1211/2		76	-	12.6	-	1.5	0.01	0.1	0.4	3.53	4.8	0.69	0.1	0.02	-	0.05	98.67	24	139	-	89	3	2	9	9.3	78	2.8	38	-	-	-	-	-
1018		76	0.2	12.7	0.3	1.6	0.01	0.11	0.7	3.43	4.5	-	0.1	-	-	0.01	99.33	41	137	83	590	19	4	34	10	-	1.1	36	-	-	-	-	-
1016/3		76	0.1	12.8	0.31	0.6	0.01	-	0.6	3.85	4.8	-	-	-	-	0.01	99.38	14	101	140	1300	9	2	19	10	-	0.3	21	-	-	-	-	-
1211		77	0.1	12.6	-	1.1	-	0.06	0.4	3.47	5.1	0.34	0.1	0.01	-	0.02	99.56	8.4	80	19	130	3	2	8	13	120	2.3	51	-	-	-	-	-
1016/1		77	-	12	0.15	0.7	-	-	0.3	3.65	4.8	-	-	-	-	-	98.99	16	128	27	93	7	2	13	10	-	0.8	53	-	-	-	-	-
1016/2		78	0.1	12.8	0.74	-	-	-	0.4	2.94	5.7	-	-	-	-	0.01	100.3	13	119	100	330	9	2	10	10	-	0.3	28	-	-	-	-	-

Table 5. *Cont.*

Sample	Rock	SiO_2	TiO_2	Al_2O_3	Fe_2O_3	FeO	MnO	MgO	CaO	Na_2O	K_2O	H_2O^+	P_2O_5	S	Cl	F	∑	Li	Rb	Sr	Ba	V	Co	Ni	Cu	Zn	Sn	Pb	Y	Nb	Zr	Hf	Ta
Sokh Massif																																
1177/11	Granodiorite	66	0.6	15.6	-	4	0.03	1.35	2.4	3.94	4	0.82	0.2	0.14	-	-	99.32	83	118	250	460	46	9	20	13	170	2.4	22	7	-	-	-	-
1177/5		68	0.5	15.3	0.13	3.3	0.05	1.42	2.3	3.81	4	0.68	0.2	0.19	0.1	-	99.61	87	146	220	630	45	8	19	15	170	2	22	9	-	-	-	-
1174	Adamellite	69	0.4	14.8	0.07	2.8	0.04	0.64	2.2	3.94	3.8	0.27	0.2	0.27	-	-	98.35	75	134	200	350	22	43	12	5.2	120	2.1	22	9	-	-	-	
1177/1		71	0.4	13.4	-	3.3	0.05	0.7	1.5	3.61	4.5	0.53	0.1	0.24	-	-	98.96	72	136	160	440	20	6	14	0	99	2.1	24	7	-	-	-	-
1177	Granite	73	0.3	13.9	0.51	2.1	0.04	0.45	1.7	3.42	4.2	0.64	0.1	0.17	-	-	100.3	53	121	160	420	18	5	13	9.2	79	2	22	10	-	-	-	-
1176		74	0.2	13.6	-	2	0.03	0.43	1.2	3.62	3.9	0.51	0.1	0.06	-	-	99.2	37	121	130	390	11	5	11	8.1	25	1.7	21	14	-	-	-	-
1177/9		74	0.1	13.3	-	2	0.03	0.1	0.7	4.37	4.6	0.21	0.2	0.05	-	-	99.52	46	134	62	230	3	3	9	6.8	32	4.3	32	4	-	-	-	-
1177/2	Aplitic granite	75	0.1	12.6	-	1.6	0.02	0.37	0.7	3.32	5.2	0.32	0.1	0.07	0.1	-	99.53	25	117	96	550	8	3	14	92	270	1.1	96	7	-	-	-	-
1177/6		75	0.1	13	0.12	0.7	0.02	0.3	0.3	2.96	6.6	0.19	0.1	0.07	-	-	99.54	14	124	89	300	3	2	7	5.7	32	1.4	37	11	-	-	-	-
1177/8		75	-	13.3	0.2	0.7	0.02	0.01	0.4	3.68	5.7	0.18	0.1	0.05	-	-	99.75	17	121	28	170	3	3	7	10	29	1.1	44	10	-	-	-	-
1175/1		77	-	12.5	-	1.4	0.01	0.13	0.3	3.39	4.7	0.58	-	0.02	-	-	99.97	24	130	29	240	3	2	10	8.9	0	1.3	33	9	-	-	-	-
1177/3		75	0.1	12.8	-	1.1	-	0.11	0.3	3.58	6	0.36	0.1	0.03	-	-	99.42	13	136	46	240	5	2	8	9.7	240	1.9	37	13	-	-	-	-

4.4. Isotope Systematics and Ages of the Massifs

The geologic age of magmatism at the EIRGD is not well constrained. The lower age limit is defined by the age of the overlying sedimentary rocks (T3–J1). The oldest manifestations of magmatic activity in the region are mafic dikes (Rb–Sr, 145–162 Ma) of the orogenic Malo-Tarynskoe gold deposit located north of the EIRGD [41]. The upper age limit of magmatism at the EIRGD is not established. The first K–Ar and Rb–Sr isotope dates obtained from granitoids of the Ergelyakh and Sokh massifs were discussed previously [6]. Based on these data, we compiled a summary of isotope ages of the rocks in these massifs determined by different isotope methods (Table 6).

Isotope ages of the EIRGD granitoids, irrespective of the determination method, vary within a wide range (97–196 Ma). This is probably due to the effects of various geological processes, including hybridism and assimilation of the enclosing rocks (sample 204, 196 ± 5 Ma) and the younging of isotope dates as a result of superposed later processes. This is discussed in detail in [6], where a conclusion is made that formation of the EIRGD granitoids occurred in the time interval 160–145 Ma with the subsequent cooling of the thermal field until 136 Ma. These results are in agreement with Ar–Ar ages of the Ergelyakh pluton (biotite, 142.9 ± 0.4 Ma [50]) and Rb–Sr ages of the Samyr and Kurdat plutons (bulk sample, 140–145 Ma [10]) and other intrusives of the Tas-Kystabyt plutonic belt [50,51].

In the interval 125–120 Ma, a new episode of tectono-magmatic activity occurred at the EIRGD as inferred from Rb–Sr dates of biotites from the Ergelyakh massif granitoids and K–Ar ages of K-feldspars from adamellites of the Sokh pluton. One of the late geological events probably took place at 110–100 Ma. These processes, likely of hydrothermal-tectonic nature, caused destruction of the isotopic systems of minerals and rocks. The possibility of a late superposed process is confirmed by young Sr biotite dates (101–106 Ma) and K–Ar plagioclase ages obtained from some EIRGD granitoid samples. The process may be synchronous with the manifestation of hydrothermal metamorphism. For example, sericite–quartz from a quartz vein with wolframite and bismuthine has a K–Ar age of 114 Ma. These events are associated with subduction-accretion processes in the rear part of the Uda-Murgal and Okhotsk-Chukotka magmatic belts of the East Asian active continental margin.

The initial Sr isotope composition (I_0) for the EIRGD granitoids varies within a wide range (0.7065–0.7093). Sr isotope heterogeneity may be due to primary and secondary reasons. Primary isotope heterogeneity (I_0 = 0.707–0.708) may be related to the heterogeneous composition of the substratum, whose melting occurred without homogenization of magma upon ascent to the emplacement level and caused local isotope microheterogeneity. Secondary isotope heterogeneity in granitoids ($I_0 > 0.708$) was likely caused by late superposed processes conditioned by a long-term tectono-magmatic evolution of the whole ore-magmatic system of EIRGD. In general, there is a reverse correlation between the Rb–Sr dates of the rocks and minerals and the I_0 value, which is indicative of the evolution of the Sr isotope composition of granitoids under conditions of a thermostatic ore-magmatic system. I_0 values obtained for the EIRGD granitoids (0.707–0.709) suggest their lower crustal protoliths, which agrees well with the Nd isotope composition ($\varepsilon Nd(T)$ = –4.4 and –2.90) of the Ergelyakh massif magmatites [52].

Table 6. Results of isotopic dating of granitoids of Ergelyakh intrusion-related gold–bismuth deposit.

Sample	Rock	K–Ar Age			Rb–Sr Age	
		Rock	Biotite	K-Feldspar	Isochron (I_0)	Biotite (I_0)
	Ergelyakh Massif					
204	Granodiorite–porphyry from endocontact zone	196 ± 5	-	-	-	-
1017	Granodiorite	-	146 ± 4	-	-	-
1181/3a	Granodiorite	-	-	-	153 ± 67 (0.7071)	105 ± 0.4 (0.7080)
1022	Granodiorite	-	-	-	157 ± 74 (0.7076)	120 ± 0.7 (0.7093)
1184	Granodiorite	-	-	-	159 (0.7073)	132 ± 9 (0.7082)
1178/5	Granodiorite	-	143 *	-	-	-
184	Granodiorite–porphyry	138	-	-	-	-
1183/3b	Adamellite	-	-	-	171 ± 28 (0.7065)	122 ± 0.4 (0.7073)
1021	Granite	110 ± 3	131 ± 1	111 ± 1	131 ± 9 (0.7083)	134 ± 2 (0.7079)
1183	Granite	-	-	-	101 ± 28 (0.7088)	98 (0.7113)
140	Granite	148	146	-	-	-
196	Fine-grained biotite granite	144 ± 4	142 ± 1	-	-	148 (0.7082)
66	Plagiogranite	157	-	-	-	-
200	Fine-grained aplitic granite	140 ± 1	-	-	-	-
89	Sericitized rock, exocontact of Au rare metal vein	125 ± 1	-	-	-	-
202	Sericite–quartz vein with wolframite and bismuthine	114 ± 5	-	-	-	-
	Sokh Massif					
1177/5	Granodiorite	-	-	-	140 ± 7 (0.7079)	107 ± 0.4 (0.7091)
1174	Adamellite	120 ± 4	158 ± 3	122 ± 2	137 ± 1 (0.7079)	142 ± 0.3 (0.7077)
1174	Plagioclase	-	-	97 ± 4	-	-
1177/9	Granite	136 ± 4	147 ± 3	131 ± 1	138 ± 17 (0.7078)	143 ± 0.4 (0.7070)

Notes: Dates were obtained at DPMGI SB RAS (Yakutsk). Isochron data obtained from mineral isochron (rock + plagioclase + K-feldspar+biotite); I_0, initial Sr composition. * Ar–Ar data [51].

5. Discussion

5.1. Petrogenesis

Petrogenetically, the EIRGD granitoids are transitional between the S- and I-types (Figure 7).

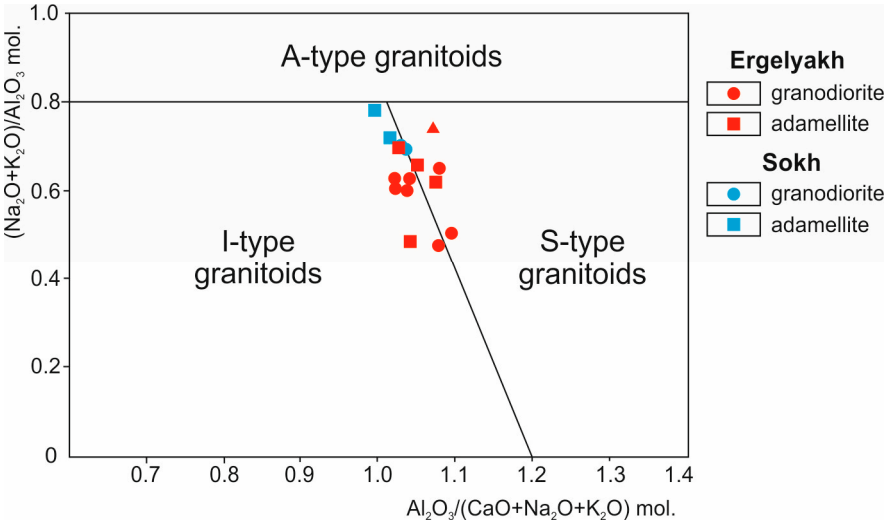

Figure 7. Petrogenetic types of the EIRGD granitoids [53].

To determine the primary sources of the EIRGD granitoids, we recalculated the data on the chemical composition of rocks according to [54] and plotted them on a discrimination diagram (Figure 8), where the fields of magma-generating substrata are outlined from the results of experimental studies [54]. Data points for granodiorites and adamellites of both massifs plot into the field of amphibolites just as those for the Sokh massif granites, whereas the Ergelyakh pluton granites fall mainly into the field of amphibolites and partly greywackes, with some altered varieties falling into the field of metapelites.

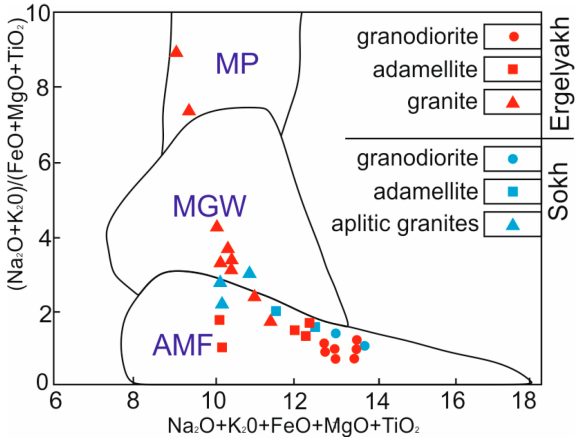

Figure 8. $(Na_2O + K_2O)/(FeO + MgO + TiO_2) – (Na_2O + K_2O + FeOT + MgO + TiO_2)$ diagram for EIRGD granitoids [54]. MP, metapelites; MGW, metagraywackes; AMF, amphibolites.

The age of protoliths calculated from the Rb–Sr model dates (Table 7) with the use of the method described in [55] varies within a narrow range (1035–1383 Ma), coinciding with their Sm–Nd model ages (1199–1322 Ma) (Table 8) [52]. Their formation was likely related to Mesoproterozoic (Riphean) geodynamic events. Figure 9 shows the plot of $^{87}Rb/^{86}Sr$ vs $^{87}Sr/^{86}Sr$. For all igneous rocks of the Ergelyakh and Sokh massifs, a positive relationship is observed between the $^{87}Rb/^{86}Sr$ and $^{87}Sr/^{86}Sr$ parameters.

Table 7. Model Rb–Sr age and parameters of protoliths for EIRGD granitoids.

Sample	Rock	$^{87}Rb/^{86}Sr$	$^{87}Sr/^{86}Sr$	I_0	$f_{Rb/Sr}$	ε_{Sr}	T_{DM}-2st
Ergelyakh Massif							
1181/3a	Granodiorite	1.422	0.710	0.707	16.19	39.56	1117
1022	Granodiorite	4.776	0.718	0.708	56.75	46.63	1109
1184	Granodiorite	4.493	0.718	0.707	53.33	42.40	1207
1181/3b	Adamellite	1.309	0.710	0.707	14.82	41.95	1136
1021	Granite	10.731	0.728	0.708	128.76	56.13	1383
196	Granite	0.38	0.709	0.708	3.59	55.00	1354
1183	Granite	9.532	0.725	0.709	114.27	30.61	1035
Sokh Massif							
1177/5	Granodiorite	3.08	0.714	0.708	36.24	50.60	1284
1174	Adamellite	1.99	0.712	0.708	23.03	47.80	1270
1177/9	Granite	10.373	0.728	0.708	124.43	49.15	1185

Notes: $f_{Rb/Sr}$ and ε_{Sr} are deviations of the $^{87}Rb/^{86}Sr$ ratio and Sr isotope ratio relative to primitive mantle reservoir in the protolith of granitoids; T_{DM}-2st is the two-stage model age of the protolith formation.

Table 8. Model Sm–Nd age and parameters of protoliths for EIRGD granitoids.

Sample	Rock	Sm	Nd	$^{147}Sm/^{144}Nd$	$^{143}Nd/^{144}Nd$	$f_{Sm/Nd}$	ε_{Nd}	T_{DM}	T_{DM}-2St
1184	Granodiorite	5.83	29.47	0.1196	0.5123	−0.39	−4.38	1317	1322
1183	Granite	4.34	16.33	0.1607	0.5125	−0.18	−2.90	2001	1199

Notes: f_{Sm-Nd} and ε_{Nd} are deviations of the $^{147}Sm/^{144}Nd$ ratio and Nd isotope ratio relative to the primitive mantle reservoir in the protolith of granitoids; T_{DM} and T_{DM}-2st are the one- and two-stage model ages of the protolith.

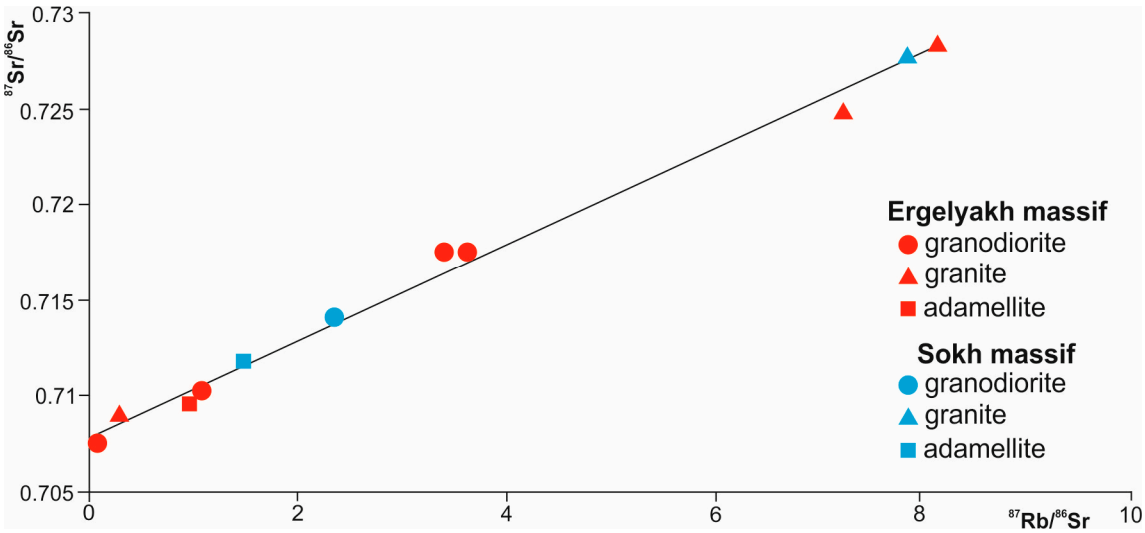

Figure 9. Rb-Sr isocron diagram for granitoids of the Ergelyakh and Sokh massifs.

Some data available on the rare elements from the Ergelyakh massif granitoids plotted on the discrimination geodynamic diagrams suggest that they were formed in an island arc or a continental arc setting (Figures 10 and 11). The new data obtained indicate that the granitoids of the Ergelyakh and Sokh massifs were formed in relation to subduction in the Uyandina-Yasachnaya volcanic arc.

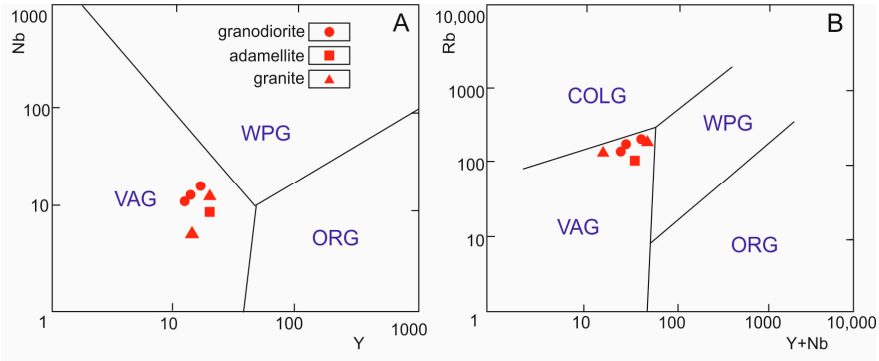

Figure 10. Discrimination (**A**) Nb–Y and (**B**) Rb–(Y + Nb) diagrams for Ergelyakh massif granitoids [56]. WPG, within-plate; VAG, volcanic island area; COLG, collisional; ORG, oceanic ridges.

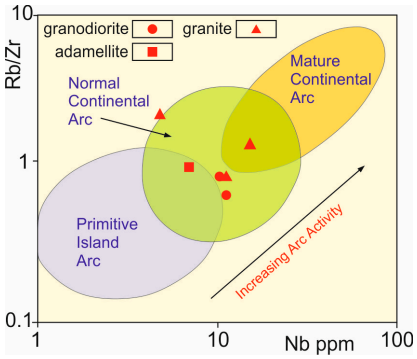

Figure 11. Discrimination Rb/Zr–Nb diagram for Ergelyakh massif granitoids [57].

5.2. Physicochemical Conditions of Granitoid Formation

The conditions of formation of the EIRGD granitoids were determined by different methods based on the chemical composition of the rocks and their minerals (biotite, feldspars). Temperatures of the melt generation based on the empirical petrochemical geothermometer [24,25] are similar for granitoids of the Ergelyakh and Sokh plutons: granodiorites, 1010–1065 °C; adamellites, 977–1033 °C; and granites, 958–985 °C (Tables 9 and 10).

Aplitic melts of the Ergelyakh pluton were formed at a higher temperature (952–980 °C) than aplitic granites of the Sokh massif (970–718 °C). Water content in the parent melt for the Ergelyakh massif granitoids, determined with a model from [25], was 2.0–5.0% (3.2 ± 0.9% for granodiorites and 3.1 ± 0.1% for adamellites). The melt for the Sokh massif granitoids contained 3.4–3.7% water. Formation of the melt for granodiorites of the Ergelyakh massif occurred at a pressure of 8.5 ± 3.6 kbar, for adamellites at 10.0 ± 1.6 kbar, and for granitoids of the Sokh massif at 11.2 kbar. Assuming that the density of the overlying rocks is 2.7g/cm^3, these pressures approximately correspond to melt formation depths of 22.9 ± 8.7 km, 27.0 ± 4.2 km, and 30.2 km, respectively. Magma ascending to the surface and its cooling-initiated crystallization of Ti-bearing phases. The highest crystallization temperatures were obtained from the Ti geothermometer [26] for granodiorites and adamellites (827–901 °C) and the lowest ones for granites and aplites (602–793 °C) of both massifs. The temperatures of rocks saturated with apatite (T_{Ap} = 630–892 °C) indicate that its crystallization began practically synchronously with Ti minerals but lasted somewhat longer. High temperatures of apatite saturation in some rocks (>900 °C) (Table 9) may be due to the presence of restitic apatites. Temperatures of zircon (T_{Zr} = 680–786 °C) and monazite (TREE = 660–851 °C) saturation indicate that these minerals were formed under conditions of decreasing magmatic melt temperature.

The rock-forming minerals crystallize within a wide range of temperatures. Biotite crystallizes at temperatures of 574–749 °C from Ti geothermometry [27] (Table 11). For one granodiorite sample (1181/3a), using a technique from [58], we determined a temperature of co-crystallization of three

garnet–biotite pairs in the range of 653–674 °C, which is in agreement with the temperature estimated from Ti geothermometer (676 °C). Similar crystallization temperatures are characteristic of quartz (623–653 °C) from granitoids of the Ergelyakh massif (Ti quartz geothermometer [59]). Some biotite grains that were modified in the course of subsolidus reactions in oxidizing conditions have lower crystallization temperatures (441–574 °C).

Table 9. Formation and crystallization temperatures of EIRGD granitoids.

Sample	Rock						Quartz	Biotite		K-feldspar–An
	T p (1)	T_{Ti}	T_{Zr}	T_{REE}	T_{Ap}	ASI	T	T	P, kbar	T
Ergelyakh Massif										
Granodiorite										
1181/3a	1036	882	771	770	837	1.11	-	676	1.82	838
1017	1018	901	749	-	876	1.08	-	638	3.08	-
1022	1035	857	786	-	895	1.03	-	661	1.95	695
1184	1023	866	-	-	765	1.04	653	682	1.67	694–727
1016	1021	868	764	-	813	1.02	-	-	-	-
1212	1065	881	-	Daika	809	1.08	-	-	-	-
1015	1024	870	-	-	697	1.05	-	-	-	-
Adamellite										
1178/4	1008	839	-	-	775	1.02	-	-	-	-
1210	1013	855	-	-	747	1.04	-	-	-	-
1181/3B	1003	852	741	743	830	1.08	623	679	1.31	743–692
1019	1033	890	-		761	1.04	-	-	-	-
Granite										
1211/3	985	792	-	-	677	1.06	-	663	1.77	483
1021	979	721	722	763	763	1.18	-	441	4.40	-
1183	973	724	712	745	814	1.12	634	574	3.71	-
1213/1	976	707	-	-	825	1.10	-	-	-	-
1211/2	965	657	682	660	892	1.08	643	-	-	-
1211	958	688	-	-	868	1.05	-	-	-	-
1020/1	971	776	-	-	869	1.19	-	-	-	-
1020/4	972	772	-	-	840	1.22	-	-	-	-
1020/3	966	761	-	-	838	1.16	-	-	-	-
Aplite										
1017/1	980	602	701	-	789	1.04	-	-	-	-
1018	968	759	-	-	874	1.08	-	-	-	-
1016/3	959	701	-	-	842	1.02	-	-	-	-
1211	958	688	-	-	868	1.05	-	-	-	-
1016/1	958	660	-	-	831	1.02	-	-	-	-
1016/2	952	679	-	-	838	1.08	-	-	-	-
Sokh Massif										
Granodiorite										
1177/11	1020	862	-	-	754	1.04	-	715	2.15	-
1177/5	1015	853	-	-	774	1.04	-	749	2.70	520
Adamellite										
1174	1006	842	-	741	846	1.01	-	709	2.01	602
1177/1	999	827	-	-	929	0.99	-	-	-	-
Granite										
1177	987	538	-	-	630	1.06	-	713	1.76	-
1176	982	793	-	768	830	1.11	-	-	-	-
1177/9	969	722	-	-	991	0.99	-	600	2.33	-
Aplitic granite										
1177/2	970	737	-	-	738	1.02	-	-	-	-
1177/6	960	688	-	-	888	1.0	-	-	-	-
1177/8	957	640	-	-	737	1.04	-	-	-	-
1175/1	718	658	-	-	786	1.12	-	-	-	-
1177/3	757	686	-	-	886	0.99	-	-	-	-

Table 10. Plagioclase–liquidus equilibrium parameters of formation of EIRGD granitoids.

Sample	Rock	An (%)	H_2O (%)	P (kbar)	T (°C)
Ergelyakh Massif					
1181/3a	Granodiorite	31	3.25 ± 0.05	10.6	1049 ± 12
1022	Granodiorite	30	3.1 ± 0.60	7.4	1010 ± 13
1184	Granodiorite	31	3.25 ± 0.15	9.1	1026 ± 14
1184	Granodiorite	41	2.35 ± 0.15	6.1	1034 ± 9
1184	Granodiorite	22	4.45 ± 0.05	12.9	1014 ± 22
1017	Granodiorite	34	2.30 ± 0.60	4.4	1015 ± 17
1017	Granodiorite	27	3.10 ± 0.60	7.1	1010 ± 23
1017	Granodiorite	24	3.45 ± 0.55	8.5	1008 ± 25
1017	Granodiorite	23	1.95 ± 0.55	3.6	1019 ± 12
1017	Granodiorite	15	4.95 ± 0.55	15.0	1004 ± 30
1211/3	Adamellite	22	2.85 ± 0.45	11.5	982 ± 27
1181/3b	Adamellite	42	2.45 ± 0.45	8.1	982 ± 16
1181/3b	Adamellite	36	3.00 ± 0.40	9.4	977 ± 17
1181/3b	Adamellite	33	3.10 ± 0.30	11.0	980 ± 16
Sokh Massif					
1177/5	Granodiorite	23	3.65 ± 0.05	11.2	1012
1174	Adamellite	26	3.4 ± 0.0	11.2	1013

Table 11. Parameters of biotite formation from EIRGD granitoids.

Sample	IV (F)	IV (Cl)	IV (F/Cl)	T °C (Ti)	P (kbar)	Buffer	T °C	Log fO_2	ΔNi–NiO	Mg#
Ergelyakh Massif										
Granodiorite										
1181/3a	2.03	–3.82	5.85	676	1.8	Ni-Ni	764	–14.95	0.29	0.39
1017	1.72	–3.28	5.01	638	3.1	Ni-Ni	743	–15.10	–1.13	0.33
1022	2.04	–3.77	5.81	661	2.0	Ni-Ni	754	–15.02	0.44	0.36
1184	1.98	–3.85	5.83	682	1.7	Ni-Ni	762	–14.96	0.34	0.38
Adamellite										
1181/3b	1.94	–4.301	5.96	679	1.3	FMQ	848	–12.97	0.51	0.43
Granite										
1211/3	1.60	–4.12	5.72	663	1.8	FMQ	829	–14.48	0.66	0.39
1021	1.75	–3.26	5.01	441	4.4	Ge-Mg	448	–19.17	6.29	0.05
1183	1.40	–3.26	4..68	574	3.7	Ni-Ni	654	–18.74	0.36	0.08
278	1.50	-	-	681	2.2	FMQ	828	–14.48	–0.69	0.39
288-g	1.46	-	-	669	1.3	Ni-Ni	749	–13.32	2.33	0.35
Sokh Massif										
Granodiorite										
1177/11	1.86	–3.47	5.34	715	2.2	Ni-NiO	756	–14.55	0.86	0.39
1177/5	1.79	–3.72	5.51	749	2.7	F MQ	842	–13.00	0.53	0.42
Adamellite										
1174	1.38	–3.74	5.12	709	2.0	F MQ	825	–14.51	–0.63	0.38
Granite										
1177/9	1.48	–3.86	5.33	600	2.3	Ni-NiO	704	–15.74	0.97	0.24
1177	1.54	–3.77	5.31	713	1.8	F MQ	806	–14.64	–0.36	0.35

Notes: Temperatures are calculated for 2 kbar pressure. IV (F), IV (Cl), and IV (F/Cl), geochemical parameters of F–OH, Cl–OH, and F–Cl exchange reactions in biotite after [31]; T °C (Ti), crystallization temperature of biotite according to [27]; P, kbar, crystallization pressure according to [30]; buffer parameters T °C, Log fO_2, ΔNi–NiO, Mg# calculated by model after [32] using MICA + program [31]. Buffer: FMQ, fayalite–magnetite–quartz; Ni–NiO, nickel–nickel; Ge–Mg, hematite–magnetite. T °C, crystallization temperature; Log fO_2, oxygen fugacity in biotite; ΔNi–NiO, oxygen fugacity relative to Ni–NiO buffer (ΔNi–NiO = LogfO_2(sample)–LogfO_2(Ni–NiO)) at given temperatures.

Crystallization temperatures of feldspars determined on the basis of the albite–orthoclase–anorthite thermometer [28] and two-feldspar thermometer [29] range widely (939–327 °C) (Table 12). This is indicative of the long history of their formation under nonequilibrium conditions during the magma evolution. Lower temperatures obtained from K-feldspar geothermometers reflect the effect of superposed processes. Plagioclase is among the first rock-forming minerals to crystallize at high

temperatures. It continues crystallizing with decreasing temperature simultaneously with later minerals (biotite, quartz). The basicity of plagioclase reduces, and at the lowest magma temperatures formation of albite begins, likely in relation to post-solidus conditions of the pluton emplacement. It is probable that crystallization of a portion of biotite and more basic plagioclase already began at the ascent of magma to the pluton emplacement level. Final crystallization of more acidic plagioclase, quartz, and K-feldspar from the melt occurred in the magma chamber with formation of plutonic bodies. Subsequent post-solidus and post-magmatic processes caused re-equilibration of the mineral composition and formation of secondary minerals (chlorite, sericite, albite).

Table 12. Formation temperatures of feldspars from EIRGD granitoids.

Sample	Rock	An (%)	SolvCalc			Stormer
			Alb	Ort	An	Alb
Ergelyakh Massif						
1181/3a	Granodiorite	31	923	870	923	838
1022	Granodiorite	30	695	695	695	644
1184	Granodiorite	31	534	534	534	568
1184	Granodiorite	18	480	480	480	518
1184	Granodiorite	22	489	489	489	530
1184	Granodiorite	41	586	586	586	620
1017	Granodiorite	15	542	497	542	565
1017	Granodiorite	24	644	644	644	618
1017	Granodiorite	27	604	604	604	606
1017	Granodiorite	34	670	670	670	663
1017	Granodiorite	37	727	727	727	694
1213 B15	Granodiorite	31	543	543	543	542
1213 B22	Granodiorite	8	442	442	442	458
1213 B27	Granodiorite	14	463	463	463	474
1213 B28	Granodiorite	13	463	463	463	470
1213 B41	Granodiorite	9	327	327	327	383
1213 B51	Granodiorite	34	939	939	939	867
1181/3B	Adamellite	33	706	720	706	692
1181/3B	Adamellite	36	739	739	739	688
1181/3B	Adamellite	42	761	761	761	743
1211/3	Adamellite	22	416	416	416	483
Sokh Massif						
1177/5	Granodiorite	23	552	670	552	520
1174	Adamellite	26	569	574	574	602

Notes: Temperatures are calculated for 2 kbar pressure.

Emplacement of granitoids of both plutons occurred at pressures of 1.3–4.4 kbar (Al–biotite barometer) [30]. Granodiorites, adamellites, and granites of the Ergelyakh massif were formed at 2.1 ± 0.6 (4), 1.31, and 2.7 ± 1.3 (4) kbar, respectively, and those of the Sokh massif at 2.4 ± 0.4 (2), 2.0, and 2.0 ± 0.4 (2) kbar (Table 11).

Partial pressure of oxygen (log fO_2) in granitoids of both massifs was estimated on bulk rock samples [33] for temperatures at the onset of crystallization (Tt2) and on biotite [31]. Values of log fO_2 were recalculated relative to Ni–NiO buffer (ΔNi–NiO) and are listed in Table 13. The ΔNi–NiO values range widely in granitoids of the Ergelyakh (–9.8 to +10.2) and Sokh (–9.2 to 1.0) massifs (Table 13). This reflects varying redox conditions of their formation. Different types of granitoids in the massifs are also characterized by varying ΔNi–NiO values. In the Ergelyakh massif, mean value of this parameter is –0.695 ± 2.44 (–3.60 to +3.26) in granodiorites, –4.8 ± 4.0 (–9.8 to –1.0) in adamellites, –1.8 ± 3.2 (–8.2 to +2.6) in granites, and –1.2 ± 6.1 (–8.2 to +10.2) in aplites. In the Sokh massif, the values are –5.8 ± 4.1 (–8.7 to –2.9) in granodiorites, –6.4 ± 3.5 (–3.9 to –8.8) in adamellites, –8.7 ± 0.5 (–8.2 to –9.3) in granites, and –5.2 ± 3.8 (–8.0 to –0.8) in aplites. In general, crystallization of granitoids of both massifs occurred

in reducing conditions, more strongly reducing in the Sokh massif. The degree of reduction increased irregularly from the early to late intrusion phases, which was likely related to the initial heterogeneity of their primary protoliths. Cooling of the melts down to the crystallization temperature of micas led to a higher degree of oxidation of a magmatic system and to an increase in ΔNi–NiO values as determined from the biotite composition (Table 13). Biotites from granodiorites of the Ergelyakh massif were formed at ΔNi–NiO equal to –0.01 ± 0.8 (–1.1 to +0.4), those from adamellites at +0.5, and from granites at +1.8 ± 2.7 (–0.7 to +6.3). Biotites from granodiorites of the Sokh massif crystallized at ΔNi–NiO equal to +0.7 ± 0.2 (+0.5 to +0.9), from adamellites at –0.6, and from granites at +0.3 ± 0.9 (–0.4 to + 1.0).

Table 13. fO_2 values for Ergelyakh and Sokh massif granitoids.

Sample	Rock	Rock		Biotite	
		Log fO_2 (T_{Ti})	ΔNi–NiO	Log fO_2 (T_{Bi})	ΔNi–NiO
Ergelyakh Massif					
1181/3a	Granodiorite	–16.098 (882)	–3.35	–14.950 (764)	0.292
1017		–11.292 (901)	1.18	–16.74 (743)	–1.134
1022		–16.826 (857)	–3.60	–15.02 (754)	0.443
1184		–16.317 (866)	3.26	–14.96 (796)	0.344
1016		–14.517 (870)	–1.54	-	-
1212		–12.138 (881)	–0.634	-	-
1015		–13.161 (870)	–0.18	-	-
1178/4	Adamellite	–17.159 (839)	–3.82	-	-
1210		–14.492 (855)	–1.22	-	-
1181/3b		–14.321 (852)	–0.99	–12.97 (848)	0.509
1177/1		–22.565 (828)	–9.75	-	-
1019		–20.783 (890)	–8.18	-	-
1211/3	Granite	–17.38 (792)	–2.79	–14.48 (829)	–0.66
1021		–13.833 (721)	2.58	–19.17 (448)	6.285
1183		–19.599 (724)	–3.41	–18.74 (654)	0.355
1211/2		–21.207 (657)	–3.20	-	-
1211		–19.780 (688)	–2.65	-	-
1213/1		–24.870 (707)	–8.241	-	-
1020/1		–15.121 (776)	–0.175	-	-
1020/4		–14.491 (772)	0.546	-	-
1020/3		–14.495 (761).	0.798	-	-
278		-	-	–14.48 (828)	–0.687
288-g		-	-	–13.32 (749)	2.333
1017/1	Aplite	–20.701 (602)	–1.003	-	-
1211/2		–26.214 (657)	–8.21	-	-
1018		–16.160 (759)	–0.82	-	-
1016/3		–16.360 (701)	0.426	-	-
1211		–24.788 (688)	–7.65	-	-
1016/1		–19.266 (660)	–1.349	-	-
1016/2		–7.174 (679)	10.207	-	-
Sokh Massif					
1177/11	Granodiorite	–21.864 (862)	–8.729	–14.55 (756)	0.86
1177/5		–16.167 (853)	–2.885	–13.00 (842)	0.53
1174	Adamellite	–17.450 (842)	–3.918	–14.51 (825)	–0.63
1177/1		–22.666 (827)	–8.828	-	-
1177	Granite	–22.882 (538)	–9.270	–14.64 (806)	–0.36
1176		–22.807 (792)	–8.22	-	-
1177/9		–24.890 (722)	–8.65	–15.74 (704)	0.97
1177/2	Aplite	–23.895 (737)	–8.026	-	-
1177/6		–18.468 (688)	–1.334	-	-
1177/8		–19.268 (640)	–0.763	-	-
1175/1		–25.961 (658)	–7.986	-	-
1177/3		–25.068 (686)	–7.879	-	-

Note: ΔNi–NiO fO_2 value relative to Ni–NiO buffer calculated for 2 kbar. Temperature in parentheses.

In general, there is a tendency toward varying oxygen fugacity during the evolution of biotites from granitoids of the massifs (r(To–ΔNi) = –0.8), which is indicative of the increasing oxidation degree of the rocks with decreasing emplacement temperature. The lowest-temperature biotites (441 °C) are characterized by the maximum ΔNi–NiO value (+6.3), which suggests that they were formed under conditions of a magnetite–hematite buffer. They are likely to be the products of re-equilibration during late geological processes.

Thus, the P-T data obtained for the granitoids of the studied massifs characterize wide variations of their temperature regime (901 to <450 °C, with consideration of late chloritization and albitization) and pressures of 2.3 ± 1.1 kbar (Ergelyakh massif) and 2.2 ± 0.4 kbar (Sokh massif) during the long emplacement period.

5.3. Mineragenic Potential

According to [30], the formation of ore occurrences associated with granitoids is controlled by the pressure conditions in the course of their emplacement. Particularly, pressure less than 1 kbar is favorable for the formation of Pb–Zn and Mo mineralization, while pressure of 1–2 kbar is responsible for Cu–Fe and Sn and 2–3 kbar for W occurrences. At pressures exceeding 3 kbar, no mineralization can form. From the Ti–biotite geobarometer data, the EIRGD granitoids were formed within a wide pressure range from 1.67 to 3.4 kbar (Table 12), and thus can be considered promising for certain types of mineralization. Mason [60] believes, however, that granitoids that initially formed at low fO_2 values can hardly be prospective of any mineralization, even with subsequently increasing oxygen fugacity. The data we obtained on oxygen fugacity in EIRGD rocks (Table 13) show that at the onset of the Ergelyakh granitoid crystallization, their parent magma was inhomogeneous in terms of oxygen fugacity (ΔNi–NiO from +3.3 to –3.6), becoming more oxidized in the period of biotite formation. Granitoids of the Sokh massif initially formed under reducing conditions (ΔNi–NiO = –8.7 to –2.9 for granitoids, –8.8 to –3.9 for adamellites, –9.3 to –8.2 for granites). On the FeO–$Fe_2O_{3\text{-log}}$ fO_2 diagram (Figure 12), data points for the EIRGD granitoids fall into fields of different mineralization types (Cu–Mo, Mo, W, Sn, and, partly, moderately reduced lithophile element Au association).

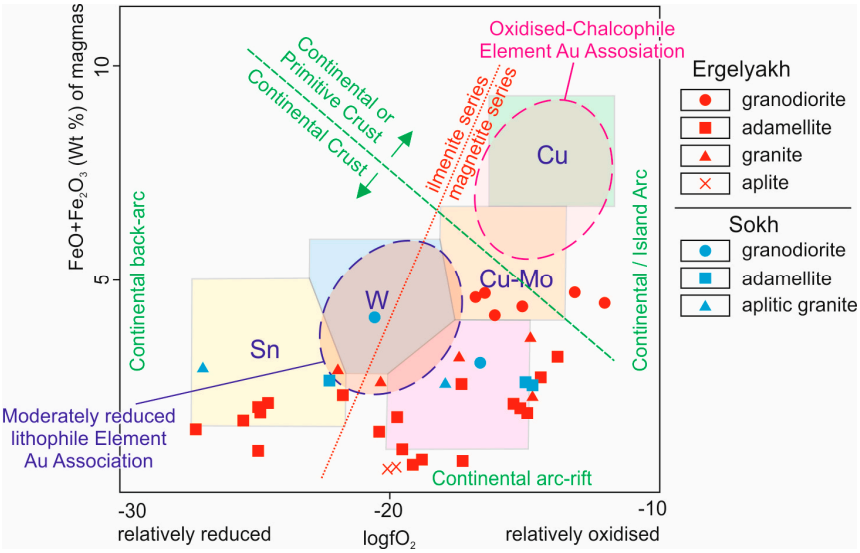

Figure 12. Schematic diagram of relationship between fractionation degree and oxidation state of magma and dominant metal paragenesis with reference to granitoids of Ergelyakh and Sokh massifs [11].

Data points for biotites on the IV(F/Cl)–IV(F) diagram are plotted into the field of rocks promising for Sn–W–Be and Cu–porphyry mineralization (Figure 13). While schematic, the discrimination diagrams presented here well illustrate the mineragenic specialties of the EIRGD.

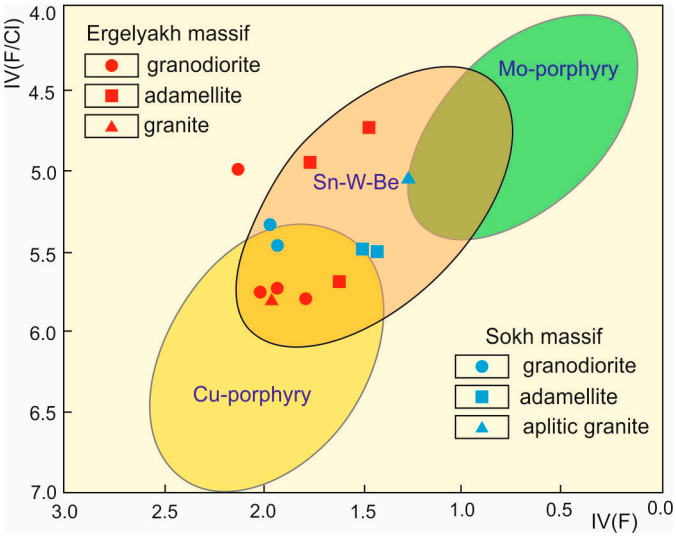

Figure 13. Discrimination diagram of IV(F/Cl)–IV(F) coordinates for biotites from Ergelyakh and Sokh massif granitoids [60].

6. Conclusions

In summary, it can be concluded that localization of the EIRGD granitoids in the Adycha-Taryn fault zone, at the boundary of the Verkhoyansk fold-and-thrust and Kular-Nera slate belts, suggests a long, multistage history of tectono-magmatic activity there. Emplacement of the granitoid massifs in the region occurred no later than 145 Ma. Various isotope systems of the rocks and minerals record at least two more stages of tectono-magmatic activity at 130–120 and 110–100 Ma. These events were likely responsible for modification of initial features of magmatic rocks and minerals and re-equilibration of their isotope systems.

Formation of granitoid magmas occurred at high temperatures (1060–950 °C) within the lower amphibolite crust, in an island-arc setting. The ages of protoliths for the EIRGD granitoids calculated from two-stage Rb–Sr and Sm–Nd models are 1109–1383 and 1199–1322 Ma, respectively. Emplacement of the Ergelyakh and Sokh massifs took place within a wide range of temperatures (900–450 °C) over a long period, taking into account late superposed processes. Parent melts for the Ergelyakh granitoids were formed in heterogeneous, more oxidizing conditions (ΔNi–NiO = +3.3 to –3.6) in contrast to granitoid melts of the Sokh massif (ΔNi–NiO = –2.9 to 9.3) that originated under reducing conditions. As the granitoid melts cooled down, a slight increase in oxygen fugacity occurred by the time of biotite crystallization in both massifs. The mineragenic potential of granitoids in both massifs seems to be similar, but owing to differences in physicochemical parameters of their formation (redox conditions), it was only partly developed in the Ergelyakh massif with the formation of small intrusion-related gold–bismuth deposits.

Author Contributions: Idea of the study conceived by A.I.Z. and V.Y.F. Methodology by A.I.Z. Treatment of data and writing the text of the paper by A.I.Z and V.Y.F. Figure drawing by M.V.K.

Funding: The reported study was done as part of the research program of DPMGI, SB RAS (project no. 0381-2019-0004).

Acknowledgments: The authors would like to thank A.I. Ivanov for preparing photomicrographs and participating in petrographic studies of the rocks. In our investigations we used thin sections made by A.G. Bakharev. We are also indebted to the reviewers for their critical comments, constructive suggestions, and valuable recommendations, which greatly improved the manuscript.

Conflicts of Interest: The authors declare no conflicts of interest.

References

1. Vikent'eva, O.V.; Prokofiev, V.Y.; Gamyanin, G.N.; Bortnikov, N.S.; Goryachev, N.A. Intrusion-related gold-bismuth deposits of North-East Russia: PTX parameters and sources of hydrothermal fluids. *Ore Geol. Rev.* **2018**, *102*, 240–259. [CrossRef]
2. Volkov, A.V.; Prokofev, V.Y.; Sidorov, A.A.; Egorov, V.N.; Goryachev, N.A.; Biryukov, A.V. Gold deposits in dikes of the Yana-Kolyma belt. *Geol. Ore Depos.* **2008**, *50*, 275–298. (In Russian) [CrossRef]
3. Volkov, A.V.; Sidorov, A.A.; Savva, N.E.; Prokofiev, V.Y.; Kolova, E.E. Prospects for the discovery of rich gold-rare metal deposits in the North-East of Russia. *Vestn. SVNTS FEB RAS* **2015**, *4*, 16–27.
4. Gamyanin, G.N. *Mineralogical and Genetic Aspects of Gold Mineralization of the Verkhoyansk–Kolyma Mesozoides*; GEOS: Moscow, Russia, 2001; p. 221. (In Russian)
5. Gamyanin, G.N.; Bortnikov, N.S.; Alpatov, V.V. *Nezhdaninskoe gold Deposit—A Unique Field of the North-East of Russia*; GEOS: Moscow, Russia, 2000; p. 226. (In Russian)
6. Gamyanin, G.N.; Goryachev, N.A.; Bakharev, A.G.; Kolesnichenko, P.P.; Diman, E.N.; Zaitsev, A.I.; Berdnikov, N.V. *Conditions of Origin and Evolution of Gold Ore Magmatic Granitoid Systems in North East Asia Mesozoids*; NEISRI FEB RAS: Magadan, Russia, 2003. (In Russian)
7. Goryachev, N.A.; Gamyanin, G.N. Gold ore Deposits of East Russia. In *Gold–Bismuth (Gold-Raremetal) Deposits of North East Russia: Types, and Exploration Perspectives*; NESC FEB RAS: Magadan, Russia, 2006; pp. 50–62. (In Russian)
8. Voroshin, S.V.; Tyukova, E.E.; Newberry, R.J.; Layer, P.W. Orogenic gold and rare metal deposits of the upper Kolyma district, Northeastern Russia: Relation to igneous rocks, timing, and metal assemblages. *Ore Geol. Rev.* **2014**, *59*, 1–24. (In Russian) [CrossRef]
9. Goryachev, N.A.; Pirajno, F. Gold deposits and gold metallogeny of Far East Russia. *Ore Geol. Rev.* **2014**, *59*, 123–151. [CrossRef]
10. Sidorov, A.A.; Volkov, A.V. Gold ore deposits in granitoids. *Dokl. Earth Sci.* **2000**, *375A*, 1382–1386. (In Russian)
11. Thompson, J.F.H.; Sillitoe, R.H.; Baker, T.; Lang, J.R.; Mortensen, J.K. Intrusion related gold deposits associated with tungsten-tin provinces. *Miner. Depos.* **1999**, *34*, 323–334. [CrossRef]
12. Lang, J.R.; Baker, T.; Hart, C.J.R.; Mortensen, J.K. An exploration model for intrusion-related gold systems. *Soc. Econ. Geol. Newsl.* **2000**, *40*, 1–15.
13. Lang, J.; Baker, T. Intrusion-related gold systems: The present level of understanding. *Miner. Depos.* **2001**, *36*, 477–489. [CrossRef]
14. Thompson, J.F.H.; Newberry, R.J. Gold deposits related to reduced granitic intrusions. *Rev. Econ. Geol.* **2000**, *13*, 377–400.
15. Hart, C.J.; Baker, T.; Burke, M. New exploration concepts for country-rock-hosted, intrusion-related gold systems: Tintina gold belt in Yukon. In *The Tintina Gold Belt: Concepts, Exploration and Discoveries*; British Columbia and Yukon Chamber of Mines: Vancouver, BC, Canada, 2000; Volume 2, pp. 145–172.
16. Hart, C.J.R.; McCoy, D.; Goldfarb, R.J.; Smith, M.; Roberts, P.; Hulstein, R.; Blake, A.A.; Bundtzen, T.K. Geology, exploration and discovery in the Tintina gold province, Alaska and Yukon. *Soc. Econ. Geol. Spec. Publ.* **2002**, *9*, 241–274.
17. Hart, C.J.R. Classifying, distinguishing and exploring for intrusion-related gold systems. The Gangue, Geological Association of Canada. *Miner. Dep. Div. Newsl.* **2005**, *87*, 4–9.
18. Hart, C.J.R. Reduced intrusion-related gold systems. *Geol. Assoc. Can. Miner. Depos. Div.* **2007**, *5*, 95–112.
19. Rozhkov, I.S.; Grinberg, G.A.; Gamyanin, G.N.; Kukhtinskiy, Y.G.; Solovyev, V.I. *Late Mesozoic Magmatism and Gold Mineralization of the Upper Indigirka District*; Nauka: Moscow, Russia, 1971; p. 238. (In Russian)
20. Gamyanin, G.N.; Nekrasov, I.Y.; Leskova, N.V.; Ryabeva, E.G. Antimonous variety of arsenopyrite: The first find. *Miner. J.* **1981**, *1*, 87–96. (In Russian)
21. Akinin, V.V.; Prokopiev, A.V.; Toro, J.; Miller, E.L.; Wooden, J.; Goryachev, N.A.; Alshevsky, A.V.; Bakharev, A.G.; Trunilina, V.A. U-Pb SHRIMP ages of granitoides from the Main batholith belt (North East Asia). *Dokl. Earth Sci* **2009**, *426*, 605–610. (In Russian) [CrossRef]
22. Zaitsev, A.I.; Nikishov, K.N.; Nenashev, N.I.; Brahfogel, F.F. Geochemistry of isotopes in xenoliths of ultrabasic and eclogitic rocks from kimberlite pipe Nude. In *Geochemistry and Mineralogy of Basites and Ultrabasites of the SIBERIAN Platform*; Springer: New York, NY, USA, 1984; pp. 80–91. (In Russian)

23. Zaitsev, A.I.; Entin, A.R.; Nenashev, N.I.; Lazebnik, K.A.; Tyan, O.A. *Geochronology and Isotope Geochemistry of Yakutia Carbonatites*; YNC SO RAN: Yakutsk, Russia, 1992; p. 248. (In Russian)
24. Rainer, V. The Abschatzung der Bildungs temperature magmatischer Schmeltzen. *Z. Geol. Wissen.* **1998**, *18*, 5–14.
25. Putirka, K.D. Thermometers and Barometers for Volcanic Systems. *Miner. Geochem.* **2008**, *69*, 61–120. [CrossRef]
26. Hayden, L.A.; Watson, E.B. Rutile saturarion in hydrous melts and its bearing on Ti-thermometry of quartz and zircon. *Earth Planet. Sci. Lett.* **2007**, *258*, 561–568. [CrossRef]
27. Henry, D.A.; Guidotti, C.V.; Thompson, J.A. The Ti-saturation surface for low-to-medium pressure metapelitic biotites: Implications for geothermometry and Ti-substitution ang mechanisms. *Am. Miner.* **2005**, *90*, 316–328. [CrossRef]
28. Wen, S.; Nekvasil, H. SOLVCALC: An interactive graphics programme package for calculating the ternary feldspar solvus and for two-feldspar geothermometry. *Comp. Geosci.* **1994**, *20*, 1025–1040. [CrossRef]
29. Stormer, J.C. A Practical two-feldspar geothermometer. *Am. Miner.* **1975**, *60*, 667–674.
30. Uchida, E.; Endo, S.; Makino, M. Relationship between solidification depth of granitic rocks and formation of hydrothermal ore deposits. *Res. Geol.* **2007**, *57*, 47–56. [CrossRef]
31. Yavuz, F. Evaluating micas in petrologic and metallogenic aspect: I–definitions and structure of the computer program MICA^{+}. *Comp. Geosci.* **2003**, *29*, 1203–1213. [CrossRef]
32. Wones, D.R.; Eugster, H.P. Stability of biotite: Experiment, theory, and application. *Am. Miner.* **1965**, *50*, 1228–1272.
33. Jayasuriya, K.D.; O'Neil, H.S.C.; Berry, A.J.; Campbell, S.J. A Mossbauer study of the oxidation of Fe in silicate melts. *Am. Miner.* **2004**, *89*, 1597–1609. [CrossRef]
34. Janousek, V.; Farrow, C.M.; Erban, V. Interpretation of whole-rock geochemical data in igneous geochemistry: Introducing Geochemical Data Toolkit (GCDkit). *J. Petrol.* **2006**, *47*, 1255–1259. [CrossRef]
35. Fridovsky, V.Y. Structures of Gold ore Fields and Deposits of Yana-Kolyma Ore Belt. In *Metallogeny of Collisional Geodynamic Settings*; Mezhelovsky, N.V., Gusev, G.S., Eds.; GEOS: Moscow, Russia, 2002; Volume 1. (In Russian)
36. Fridovsky, V.Y. Structural control of orogenic gold deposits of the Verkhoyansk-Kolyma folded region, northeast Russia. *Ore Geol. Rev.* **2018**, *103*, 38–55. [CrossRef]
37. Nokleberg, W.J.; Bundtzen, T.K.; Dawson, K.M.; Eremin, R.A.; Goryachev, N.A.; Koch, R.D.; Ratkin, V.V.; Rozenblum, I.S.; Shpikerman, V.I.; Frolov, Y.F.; et al. *Significant Metalliferous Lode Deposits and Placer Districts for the Russian Far East, Alaska, and the Canadian Cordillera*; U.S. Geological Survey: Reston, VI, USA, 1697; pp. 96–513.
38. Bortnikov, N.S.; Gamyanin, G.N.; Vikent'eva, O.V.; Prokof'ev, V.Y.; Prokopiev, A.V. The Sarylakh and Sentachan gold–antimony deposits, Sakha Yakutia: A case of combined mesothermal gold–quartz and epithermal stibnite ores. *Geol. Ore Depos.* **2010**, *52*, 339–372. (In Russian) [CrossRef]
39. Parfenov, L.M.; Berzin, N.A.; Hanchuk, A.I.; Badarch, G.; Belichenko, V.G.; Bulgatov, A.N.; Dril, S.I.; Kirillova, G.L.; Kuzmin, M.I.; Nokleberg, U.; et al. A model for the formation of orogenic belts in Central and Northeast Asia. *Russ. J. Pac. Geol.* **2003**, *22*, 7–41. (In Russian)
40. Zaitsev, A.I.; Fridovsky, V.Y.; Kudrin, M.V. Intensive formation parameters and mineragenic potential of the granitoids of the Kurdat and Samyr massifs, Tas-Kystabyt magmatic belt of the Verkhoyansk-Kolyma folded region. *Russ. J. Domes. Geol.* **2017**, *5*, 80–89. (In Russian)
41. Zaitsev, A.I.; Fridovsky, V.Y.; Vernikovskaya, A.E.; Kudrin, M.V.; Yakovleva, K.Y.; Kadilnikov, P.I. Rb-Sr isotopic study of basites of the dyke complex of the Taryn ore-magmatic system (Northeast Russia). *Russ. J. Domes. Geol.* **2018**, *5*, 50–61. (In Russian)
42. Fridovsky, V.Y.; Gamyanin, G.N.; Polufuntikova, L.I. Gold quartz and antimony mineralization in the Maltan deposit in northeast Russia. *Russ. J. Pac. Geol.* **2014**, *8*, 276–287. [CrossRef]
43. Fridovsky, V.Y.; Gamyanin, G.N.; Polufuntikova, L.I. The structure, mineralogy, and fluid regime of ore formation in the polygenic Malo-Taryn gold field, northeast Russia. *Russ. J. Pac. Geol.* **2015**, *9*, 274–286. [CrossRef]
44. Gamyanin, G.N.; Fridovsky, V.Y.; Vikent'eva, O.V. Noble-metal mineralization of the Adycha–Taryn metallogenic zone: Geochemistry of stable isotopes, fluid regime, and ore formation conditions. *Russ. Geol. Geophys.* **2018**, *59*, 1271–1287. (In Russian) [CrossRef]

45. Gamyanin, G.N.; Goncharov, V.I.; Goryachev, N.A. Gold-rare metal deposits of Northeast Russia. *Geol. Pac. Ocean* **2000**, *15*, 619–636.
46. Lykhina, L.I.; Prokof'ev, V.Y.; Gamyanin, G.N. Formation conditions for arsenic mineral assemblages of gold-rare metal deposits of Yakutia. In *Geodynamics, Magmatism and Minerageny of Continental Margins in the North Pacific*; NEISRI FEB RAS: Magadan, Russia, 2003; pp. 109–111. (In Russian)
47. Goldfarb, R.J.; Taylor, R.; Collins, G.; Goryachev, N.A.; Orlandini, O.F. Phanerozoic continental growth and gold metallogeny of Asia. *Gondwana Res.* **2014**, *25*, 48–102. [CrossRef]
48. Green, T.H. Garnet in Silicic Liquids and Its Possible Use as a P-T Indicator. *Contrib. Mineral. Petrol.* **1977**, *65*, 59–67. [CrossRef]
49. Stavrov, O.D. *Geochemistry of Lithium, Rubidium, Cesium in the Magmatic Process*; NEDRA: Moscow, Russia, 1978; p. 400. (In Russian)
50. Layer, P.W.; Newberry, R.; Fujita, K.; Parfenov, L.; Trunilina, V.; Bakharev, A. Tectonic setting of the plutonic belts of Yakutia, northeast Russia, based on $^{40}Ar/^{39}Ar$ geochronology and trace element geochemistry. *Geology* **2001**, *29*, 167–170. [CrossRef]
51. Prokopiev, A.V.; Borisenko, A.S.; Gamyanin, G.N.; Pavlova, G.G.; Fridovsky, V.Y.; Kondrat'eva, L.A.; Anisimova, G.S.; Trunilina, V.A.; Ivanov, A.I.; Travin, A.V.; et al. Age constraints and tectonic settings of metallogenic and magmatic events in the Verkhoyansk–Kolyma folded area. *Russ. Geol. Geophys.* **2018**, *59*, 1237–1253. [CrossRef]
52. Zaitsev, A.I.; Bakharev, A.G.; Prokopyev, A.V. Physico-chemical parameters of the formation of gold-bearing and tin-silver-bearing igneous complexes of the Taryn ore-magmatic node (North-East Yakutia). In *Geology and Mineral Resources of the North-East of Russia, Proceedings of the All-Russian Scientific-Practical Conference, Yakutsk, Russia, 2–4 April 2013*; IPK NEFU: Yakutsk, Russia, 2013; Volume I, pp. 194–198. (In Russian)
53. Maeda, J. Opening of the Kuril Basin deduced from the magmatic history of Central Hokkaido, northern Japan. *Tectonophysics* **1990**, *174*, 235–255. [CrossRef]
54. Patino Douce, A.E. What do experimenrs tell us about the relative contributions of crust and mantle to the origin of granitic magmas? *Geol. Soc.* **1999**, *168*, 55–75. [CrossRef]
55. Muller, A.; Mezger, K.; Schenk, V. Crystal age domains and the Continental Crust in the Mozamique Belt of Tanzania: Combined Sm-Nd, Rb-Sr, and Pb-Pb Isotopic Evidence. *J. Petrol.* **1998**, *12*, 279–288.
56. Pearce, J.A.; Harris, N.; Tindle, A.G. Trace element discrimination diagrams for the tectonics interpretation of Granitic rocks. *J. Petrol.* **1984**, *25*, 55–75. [CrossRef]
57. Rao, D.R.; Sharma, R. Arc magmatism in eastern Kumaun Himalaya, India: A study based on geochemistry of granitoid rocks. *Island Arc.* **2011**, *20*, 500–519.
58. Bhattacharya, A.; Mohanty, L.; Maji, A.; Sen, S.K.; Raith, M. Non-ideal mixing in the phlogopite–annite binary: Constraints from experimental data on Mg–Fe partitioning and reformulation of the biotite–garnet geothermometer. *Contrib. Miner. Petrol.* **1992**, *111*, 87–93. [CrossRef]
59. Huang, R.; Audetat, A. The titanium-in-quartz (TitaniQ) thermobarometer: A critical examination and re-calibration. *Geoch. Cosm. Acta.* **2012**, *84*, 75–89. [CrossRef]
60. Mason, D.R. Compositions vatiations in ferromagnesin minerals from porphyry copper-generating and barren intrusions of the western Higlands, Papua New Guinea. *Econ. Geol.* **1978**, *73*, 878–890. [CrossRef]